Cell

Endogenous Nuclear RNAi Mediates Behavioral Adaptation to Odor

Bi-Tzen Juang,[1] Chen Gu,[1,2] Linda Starnes,[1,3] Francesca Palladino,[4] Andrei Goga,[1] Scott Kennedy,[5] and Noelle D. L'Etoile[1,*]

[1]Departments of Cell & Tissue Biology and Medicine, University of California, San Francisco, 513 Parnassus Avenue, San Francisco, CA 94143-0512, USA

[2]Amunix, Inc., 500 Ellis Street, Mountain View, CA 94043, USA

[3]Chromatin Structure and Function Group, NNF Center for Protein Research, Faculty of Health Sciences, University of Copenhagen, Blegdamsvej 3B, Room 4.3.07, 2200 Copenhagen N, Denmark

[4]École Normale Supérieure de Lyon, CNRS, Molecular Biology of the Cell Laboratory/ UMR5239, Université Claude Bernard Lyon, 69007 Lyon, France

[5]Laboratory of Genetics, University of Wisconsin-Madison, Madison, WI 53706, USA

*Correspondence: noelle.letoile@ucsf.edu

http://dx.doi.org/10.1016/j.cell.2013.08.006

SUMMARY

Most eukaryotic cells express small regulatory RNAs. The purpose of one class, the somatic endogenous siRNAs (endo-siRNAs), remains unclear. Here, we show that the endo-siRNA pathway promotes odor adaptation in *C. elegans* AWC olfactory neurons. In adaptation, the nuclear Argonaute NRDE-3, which acts in AWC, is loaded with siRNAs targeting *odr-1*, a gene whose downregulation is required for adaptation. Concomitant with increased *odr-1* siRNA in AWC, we observe increased binding of the HP1 homolog HPL-2 at the *odr-1* locus in AWC and reduced *odr-1* mRNA in adapted animals. Phosphorylation of HPL-2, an in vitro substrate of the EGL-4 kinase that promotes adaption, is necessary and sufficient for behavioral adaptation. Thus, environmental stimulation amplifies an endo-siRNA negative feedback loop to dynamically repress cognate gene expression and shape behavior. This class of siRNA may act broadly as a rheostat allowing prolonged stimulation to dampen gene expression and promote cellular memory formation.

INTRODUCTION

RNA interference (RNAi) has been exploited as a powerful experimental tool in both somatic and germ cells for over a decade (Fire et al., 1998), and organisms ranging in complexity from yeast to humans produce a range of endogenous small RNAs of 20–30 nucleotides in length. Although it is apparent that almost all cells of an organism are actively engaged in some form of endogenous RNAi, its role, particularly in somatic cells, remains unclear (reviewed in Ketting, 2011; Ghildiyal and Zamore, 2009).

Endogenous small RNAs are grouped into three classes according to their biosynthetic origin and the proteins they bind: piwi-RNAs (piRNAs), micro RNAs (miRNAs), and endogenous small interfering RNAs (endo-siRNAs). piRNAs and miRNAs are encoded by genes, whereas in *C. elegans*, endo- siRNAs are produced by RNA-dependent RNA polymerases that use thousands of cellular messenger RNAs (mRNAs) as templates to produce antisense small RNAs (Ghildiyal and Zamore, 2009; Ketting, 2011; Gent et al., 2010; Gu et al., 2009). Small RNAs have been linked to synaptic function and memory formation in mammals (McNeill and Van Vactor, 2012). For instance, the microRNA miR134 was shown to repress context-dependent fear learning and long-term potentiation in mice (Gao et al., 2010), and a piRNA has been shown to promote long-term synaptic facilitation of cultured *Aplysia* sensory neurons (Rajasethupathy et al., 2012). However, the extent to which small RNAs couple environmental stimuli to synaptic plasticity and the mechanism by which small RNAs regulate experience-induced behavioral changes remain a mystery.

Prolonged odor exposure induces a form of behavioral plasticity termed adaptation. *C. elegans* is innately attracted to food-related odors, but the attraction is diminished if starvation accompanies the odor. The resulting odor-adapted state lasts until the animal is fed (Colbert and Bargmann, 1997; Lee et al., 2010). Odor sensation (Bargmann et al., 1993) and adaptation (L'Etoile et al., 2002) occur within the olfactory sensory neuron that is referred to as AWC. Whereas odor sensation requires the guanylyl cyclase (GC) ODR-1, odor adaptation requires downregulation of ODR-1 (L'Etoile and Bargmann, 2000). Decreased intracellular cGMP, in part, drives the cGMP-dependent protein kinase EGL-4 into the AWC nucleus (O'Halloran et al., 2012). Once in the nucleus, EGL-4 is both necessary and sufficient to induce long-lasting odor adaptation (Lee et al., 2010). The mechanism by which nuclear EGL-4 triggers long-lasting odor adaptation is not known.

Small RNAs can regulate gene expression in both the cytoplasm and nucleus. For instance, miRNAs and siRNAs act as guides to target mRNAs for repression in the cytoplasm (reviewed in Ketting, 2011; Ghildiyal and Zamore, 2009). piRNAs and siRNAs can enter nuclei to trigger cotranscriptional gene silencing (nuclear RNAi) (Guang et al., 2008; Le Thomas et al.,

2013). During nuclear RNAi in *C. elegans*, the Argonaute (Ago) NRDE-3 shuttles siRNAs into the nucleus, where it binds nascent transcripts that exhibit sequence complementarity to NRDE-3-associated siRNAs (Guang et al., 2008; Guang et al., 2010). NRDE-3 recruits the conserved nuclear protein NRDE-2 and two nematode-specific proteins, NRDE-1 and perhaps NRDE-4, to RNAi-targeted nascent transcripts to inhibit RNA polymerase II (RNAP II) elongation (Guang et al., 2010; Burkhart et al., 2011). In addition, genes targeted for silencing by the nuclear RNAi pathway accumulate the repressive chromatin mark, H3K9me3 (Guang et al., 2010; Burton et al., 2011). In the *C. elegans* germline, piRNAs and siRNAs trigger nuclear RNAi at thousands of genomic loci (Claycomb et al., 2009; Gu et al., 2009; Ashe et al., 2012; Lee et al., 2012; Shirayama et al., 2012), and the silencing effects can endure for more than five generations (Vastenhouw et al., 2006; Buckley et al., 2012). When nuclear RNAi is disabled, *C. elegans* germlines lose their immortal character (Buckley et al., 2012).

In this paper, we examine the role of RNAi in neurons. Four lines of evidence indicate that, in the AWC olfactory sensory neurons of adult-behaving *C. elegans*, endogenous RNAi promotes odor adaptation by repressing the *odr-1* gene. First, we show that the nuclear RNAi Ago NRDE-3 is required in the AWC neuron to promote adaptation. Second, NRDE-3 coimmunoprecipitates (coIPs) *odr-1*-directed endo-siRNAs, and in adapted animals, we find increased levels of NRDE-3-bound *odr-1* siRNA. Third, odor exposure diminishes the levels of *odr-1* mRNA. Fourth, in odor adaptation, HPL-2, a heterochromatin-binding protein, is loaded onto the *odr-1* locus. Additionally, we find that phosphorylation of HPL-2 at sites that are in vitro targets of the odor-responsive kinase EGL-4 is both necessary and sufficient to promote odor adaptation in the AWC neurons of an intact animal. Our work indicates a mechanism by which environmentally relevant experiences may regulate gene expression, thereby shaping behavior in a specific and dynamic fashion.

RESULTS

The Nuclear RNAi Argonaute NRDE-3 Is Required in the AWC Sensory Neuron for Odor Adaptation

C. elegans is innately attracted to the odor, butanone. Attraction is assessed by the chemotaxis assay shown in Figure 1A, which allows quantification of the behavior in the form of a chemotaxis index (CI) (Bargmann et al., 1993). Naive wild-type animals exhibit a high CI to butanone, which decreases after 80 min of butanone exposure in the absence of food (Colbert and Bargmann, 1995). This experience-dependent decrease in CI is termed long-term olfactory adaptation. If the adapted CI is greater than one half of the naive CI, a strain is considered adaptation defective.

To investigate the role of small RNAs in long-term olfactory adaptation, we examined butanone adaptation in strains defective for major pathways producing RNAi in the soma, including the microRNA, exogenous RNA (exo-RNAi), and endogenous RNAi pathways. Animals lacking Dicer (DCR-1) were defective for adaptation (Figure 1B). Dicer, an RNAase III, processes double-stranded (dsRNA) into small noncoding RNAs (Grishok et al., 2001; Knight and Bass, 2001; Duchaine et al., 2006) that feed into the microRNA, exo-, and endo-siRNA interference pathways (Grishok et al., 2001; Knight and Bass, 2001; Grishok et al., 2005). These data suggest that Dicer-mediated processing of dsRNA is required for adaptation. By contrast, the adapted CI of strains bearing mutations in the pri-miRNA-processing RNase III enzyme Drosha, DRSH-1 (Denli et al., 2004), the miRNA-binding Ago, ALG-2 (Vasquez-Rifo et al., 2012), or the exo-RNAi pathway Ago, RDE-1 (Tabara et al., 1999), were not significantly different from the CI of wild-type controls (Figures 1B and S2 available online). These data suggest that, if Dicer-mediated dsRNA processing is required for butanone adaptation, microRNAs or the exoRNAi pathway are unlikely to mediate this process.

MUT-7, a putative 3′ to 5′ exonuclease, is required for accumulation of endogenous 22 nucleotide siRNAs that bind the WAGO clade of Agos (Yigit et al., 2006; Lee et al., 2006; Gu et al., 2009) and accumulation of 26 nucleotide siRNAs (Zhang et al., 2011), as well as transposon and transgene silencing, exogenous RNAi, and proper chromosome segregation (Ketting et al., 1999; Tabara et al., 1999; Dernburg et al., 2000; Tops et al., 2005). MUT-7 is also required for nuclear accumulation of NRDE-3 (Guang et al., 2008). HPL-2 is one of two *C. elegans* homologs of Heterochromatin Protein 1 (HP1) (Couteau et al., 2002). HPL-2 is involved in multiple cellular events, including gene regulation and DNA replication and repair (Couteau et al., 2002; Coustham et al., 2006; Black and Whetstine, 2011), as well as transgene silencing and piRNA-mediated gene silencing in the gonad (Grishok et al., 2005; Burkhart et al., 2011; Ashe et al., 2012; Buckley et al., 2012; Shirayama et al., 2012). Strains that lacked MUT-7 or HPL-2 were defective for butanone adaptation (Figure 1B). These results suggest that heterochromatin and possibly small RNAs promote odor adaptation downstream of Dicer.

Using *mut-7* and *hpl-2* promoter fusions to drive expression of GFP-tagged MUT-7 or HPL-2, respectively, we observed GFP expression in many cells, including both AWCs (Figure 1C). To determine whether MUT-7 and HPL-2 act in the AWC neurons, the site of odor sensation and adaptation, we asked whether cell-specific expression of MUT-7 and HPL-2 could rescue the odor adaptation defect of each corresponding mutant strain. Expressing MUT-7 or HPL-2 solely within the AWC neurons (from the AWC-specific *ceh-36*^{prom3} promoter [Etchberger et al., 2007]) of the respective mutant strain rescued its adaptation defects (Figure 1D). These data indicate that MUT-7 and HPL-2 act within AWC neurons to promote odor adaptation.

These factors could be required at the time of odor exposure or developmentally. To distinguish between these possibilities, we used the heat shock promoter p*hsp-16.2* (Stringham et al., 1992) to express each factor in the adult immediately prior to odor exposure. Heat-shock-driven expression restored adaptation to the *mut-7* and *hpl-2* strains (Figure 1E). Consistent with a requirement in the adult, neither morphology nor cell fate of the AWC was altered by loss of HPL-2 or MUT-7 (Figure S1B and Table S1). Together, these results indicate that the adaptation defects of *mut-7*- and *hpl-2*-deficient animals are not due to developmental defects.

To address whether MUT-7 and HPL-2 act in the same molecular pathway, we created *mut-7;hpl-2* and control

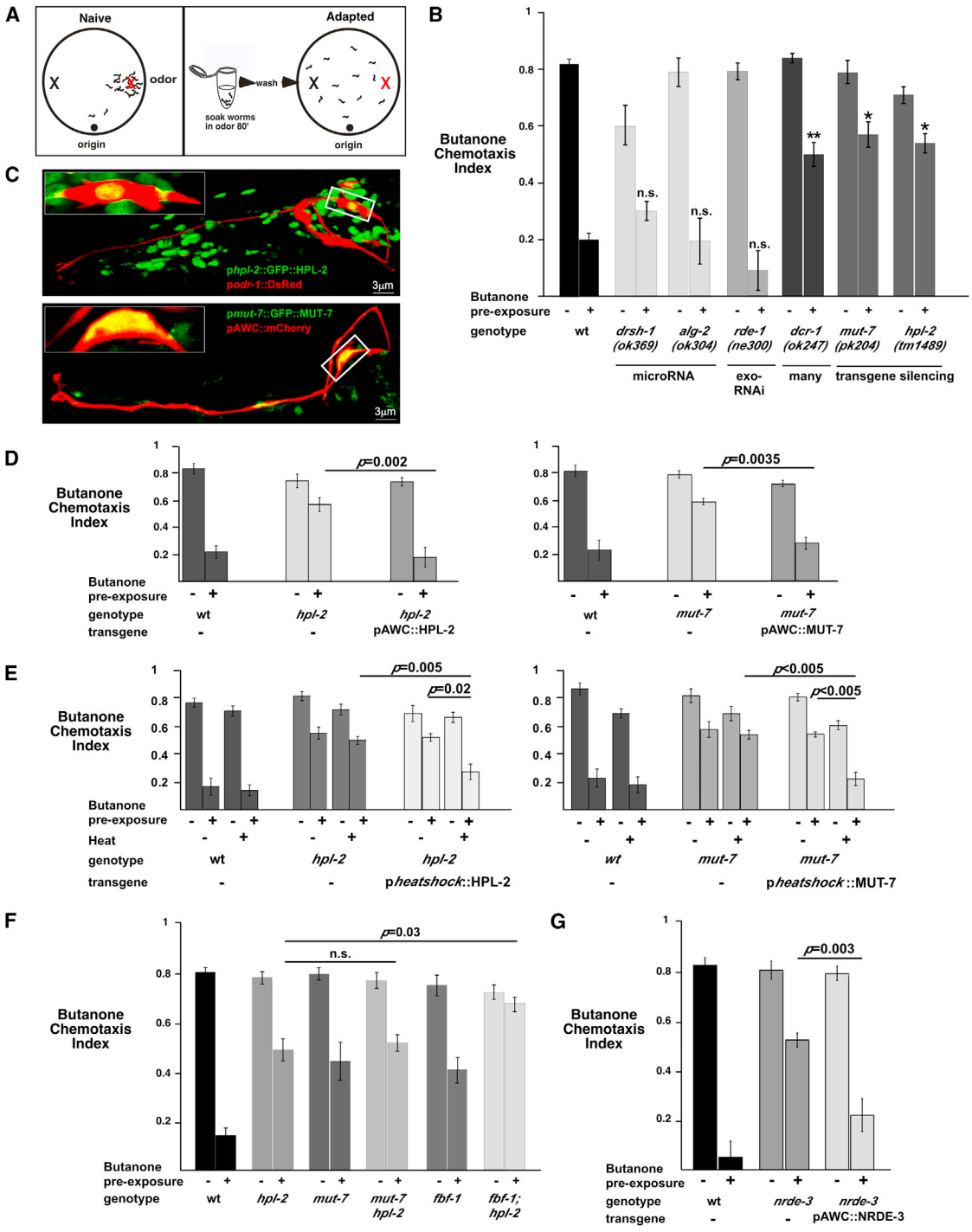

Figure 1. HPL-2 and MUT-7 Act at the Time of Odor Exposure in the AWC Neurons to Promote Adaptation to Butanone

(A) Olfactory adaptation paradigm. Animals exposed to buffer alone (naive) or butanone (adapted) for 80 min are placed at the "origin" of an agar-lined 10 cm Petri dish. Butanone is placed at the red and ethanol at the black "X." Sodium azide (to paralyze the worms) was also placed at each "X." Animals roam plates 2 hr before counting. The CI is calculated by subtracting the number of animals at the diluent from the number at the odor and dividing this by the number of animals that left the origin.

(B) Initial screen of mutant strains defective for siRNA pathways. Bars represent mean CIs of strains of the indicated genotype that had either been incubated with buffer (−) or buffer-diluted butanone (+) for 80 min. Bars for wild-type represent the mean CI of pooled controls for all the strains. All error bars are SEM. The side-by-side comparisons of each strain with wild-type controls are shown in Figure S1A. ** = $p < 0.005$, * = $p < 0.05$, and "n.s." = $p > 0.05$. Unless otherwise noted, all tests were two-tailed Student's t test, and all assays were performed on separate days with >100 animals per assay. *drsh-1*, *alg-2*, *dcr-1*: n = 4; *rde-1* mut-7: n = 6; *hpl-2*: n = 5.

(legend continued on next page)

Table 1. Olfactory Adaptation Requires a Nuclear RNAi Pathway

Gene (Allele)	Gene Function	Butanone Adaptation[a]
dcr-1(ok247)[b]	RNase III nuclease	defective
rde-4(ne337)	double-stranded RNA binding	defective
drsh-1(ok369)	RNase III nuclease	partially chemotaxis defective
rrf-1(pk1417)	RNA-dependent RNA polymerase	wild-type
rrf-2(ok210)	RNA-dependent RNA polymerase	wild-type
rrf-3(pk1426)	RNA-dependent RNA polymerase	partially defective
drh-1(tm1329)	RNA helicase (RIG-I)	wild-type
drh-2(ok951)	RNA helicase (RIG-I)	defective
drh-3(ne4253)	RNA helicase	chemotaxis defective
rde-3(ne3364)	β-nucleotidyl transferase	defective
mut-7(pk204)	3′-5′ exonuclease	defective
rde-1(ne300)	exo-RNAi Argonaute	wild-type
ergo-1(gg98)	Argonaute	wild-type
alg-2(ok304)	microRNA Argonaute	wild-type
quintuple	5 Argonautes	wild-type
MAGO12	12 Argonautes	defective
nrde-3(gg66)	nuclear RNAi Argonaute	defective
nrde-2(gg91)	NRDE-3 binding nuclear factor	defective
nrde-1(gg88)	NRDE-2/3-chromatin associated	defective
hpl-2(tm1489)	histone H3 lysine 9 trimethyl binding (HP1)	defective

[a]Behavioral assays are shown in Figure S1A.
[b]Heterozygous animals are marked with hT2::GFP(I,III).

fbf-1;hpl-2 double-mutant animals. We found that the ability of *hpl-2* or *mut-7* single-mutant animals to adapt to odors was similar to the ability of *mut-7;hpl-2* double-mutant animals (Figure 1F), but the adaptation defects of *hpl-2* were enhanced in the *fbf-1;hpl-2* double-mutant strain. These data indicate that MUT-7 and HPL-2 likely act in the same pathway within AWC to promote odor adaptation at the time of odor exposure.

To probe the involvement of nuclear RNAi in adaptation, we examined the nuclear Ago, NRDE-3. NRDE-3 interacts with a subset of endo-22GRNAs and shuttles them into the nucleus, where they direct cotranscriptional gene silencing (Guang et al., 2008). NRDE-3 is expressed in the AWC neurons (B.-T.J. and N.D.L., unpublished data), and the NRDE-3 null (*nrde-3(gg66)*) was unable to adapt to butanone (Figure 1G). These adaptation defects were rescued by expressing NRDE-3 solely in the AWC neuron (Figures 1G and S1C), demonstrating that the nuclear RNAi Argonaute NRDE-3 acts in AWC to promote odor adaptation.

To better characterize the nuclear RNAi pathway, we surveyed adaptation in siRNA-defective strains that were deemed chemotaxis proficient (Table 1 and Figure S1A). In *C. elegans*, RNAi can be broken down into three steps: trigger processing, amplification, and silencing (reviewed in Pak et al., 2012). We found that trigger processing factors, Dicer and its partner RDE-4 (Tabara et al., 2002; Duchaine et al., 2006), are required for adaptation. The siRNA-amplifying RNA-dependent RNA polymerase (RdRP), RRF-3 (Simmer et al., 2002), was partially required as *rrf-3(pk1426)* animals failed to adapt in five out of eight trials. The silencing factor NRDE-3, along with its nuclear complex of NRDE-2 (Guang et al., 2010) and NRDE-1 (Burkhart et al., 2011), were each required. These results suggest that adaptation requires trigger processing, possibly RdRP amplification, and nuclear Ago-mediated silencing.

Biochemical and genetic analyses have implicated additional factors in RNAi. Of the many factors shown to associate with Dicer, DRH-2 (a Dicer-related DExH-box helicase [Tabara et al., 2002]) and RDE-3 (a β-nucleotidyl transferase) (Duchaine et al., 2006) were required for adaptation. Taken as a whole, our genetic analysis indicates that the nuclear RNAi pathway is likely to act in the AWC neuron to promote odor adaptation downstream of DCR-1/RDE-4-mediated small RNA production.

odr-1 mRNA Decreases in Odor-Adapted Animals

To identify a target for siRNA in adaptation, we used quantitative real-time PCR to probe endo-22GRNAs that map to AWC-expressed genes (see Supplemental Information). We found that the *odr-1*-derived 22GRNAs, odr-1.6 and odr-1.7, as well as the *unc-40*-derived 22GRNA, unc-40.2, gave the most robust signals. *odr-1* encodes a GC whose downregulation is required for odor adaptation (L'Etoile and Bargmann, 2000), and *unc-40* encodes an axon guidance and synaptogenesis factor

(C) HPL-2 and MUT-7 are expressed in AWCs. Fluorescent confocal images of wild-type animals expressing the putative *hpl-2* (top) or *mut-7* (bottom) promoters driving GFP-tagged versions of each protein. AWC is marked with *ceh-36*^{prom3} promoter driving mCherry. Anterior is at the left for both images. Figure S1B is associated with this panel.
(D) Expression of HPL-2 or MUT-7 in AWC rescued the adaptation defects of each mutant. HPL-2 (left graph, third pair of bars) or GFP-tagged MUT-7 (right graph, third pair of bars) was expressed in AWC from p*ceh-36*^{prom3} in *hpl-2(tm1489)* or *mut-7(pk204)*, respectively. **p = 0.002, *p = 0.0035, and n > 5 for each.
(E) Expression of HPL-2 or MUT-7 at the time of odor exposure rescued adaptation defects. *hpl-2(tm1489)* (left) or *mut-7(pk204)* (right) transgenic for the respective cDNA under the control of the heat shock promoter (p*hsp16-2)* were heated (+) 1 hr before odor exposure. Heat-treated animals' exposed CI's were significantly different from either before heating (p = 0.02, *hpl-2*; p < 0.005, *mut-7*) or from nontransgenic animals that had been heated (p = 0.005, *hpl-2*; p < 0.005, *mut-7*), n > 5 for each.
(F) HPL-2 and MUT-7 act in the same genetic pathway for adaptation. Mean naive (−) and exposed (+) CIs of animals of the indicted genotype. The adaptation defects of the *fbf-1(ok91)* strain are due to loss of the translational control pathway (Kaye et al., 2009) that acts in parallel with *hpl-2*.
(G) Expression of NRDE-3 in AWC rescued the adaptation defects of the *nrde-3* mutant strain. Mean CI of naive (−) and exposed (+) wild-type, *ndre-3(gg66)*, and NRDE-3 expressed in AWC (p*ceh-36*^{prom3}) of the *nrde-3(gg66)* mutant strain. Figure S1D is associated with this figure.
Error bars for each panel are SEM.

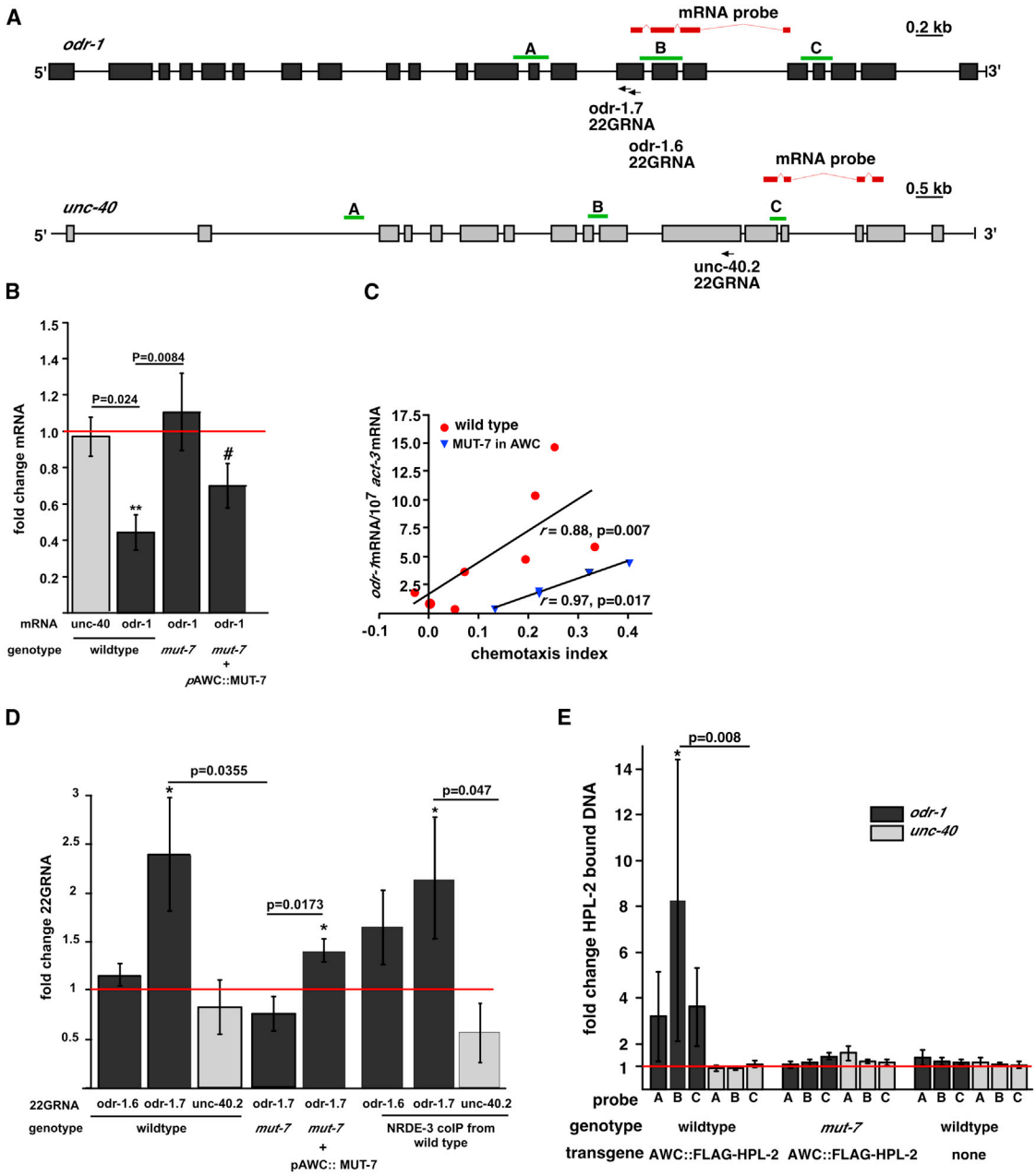

Figure 2. Prolonged Odor Stimulation Dynamically Regulates *odr-1*-Derived 22G RNAs, Association of HPL-2 with the *odr-1* Locus, and Levels of *odr-1* mRNA

(A) Diagram of the *odr-1* and *unc-40* genes. The *odr-1* and *unc-40* 22GRNAs examined are indicated with arrows below the gene. The PCR amplicons for ChIP-qPCR are in green. PCR amplicons for mRNA analysis are in red.

(B) Prolonged odor exposure decreases *odr-1* mRNA levels. Bars represent the mean fold change in *unc-40* (gray) or *odr-1* (black) mRNA level as a function of odor exposure (adapted/naive). RNA from animals of the indicated genotype was normalized to *act-3* mRNA. The red line indicates "no change," and the significance of the difference between a sample and "no change" was assessed using a two-tailed Wilcox signed rank test. ** indicates that median of sample and "no change" are different; $p < 0.005$. # indicates a difference of $p = 0.034$ (nonparametric, pair-wise comparison) in medians between the naive and adapted values of the mRNA. p values displayed are from two-tailed Mann-Whitney test of medians. Chemotaxis behavior for each population and the individual data points for each pair are shown in Figure S2A. Error bars represent SEM, and $n > 3$.

(C) Chemotaxis behavior correlates with the level of *odr-1* mRNA in butanone-adapted animals. The butanone CI of odor-exposed animals was compared with their *odr-1* mRNA level (mRNA levels normalized to *act-3* mRNA). Red circles indicate wild-types, and blue triangles indicate *mut-7(pk204)* animals expressing MUT-7 solely within the AWC neurons. r is Pearson's correlation coefficient, and p is from a two-tailed Student's t test (wild-type, $n = 8$; AWC MUT-7 rescue, $n = 5$).

(D) Prolonged odor exposure increases NRDE-3-bound *odr-1* 22GRNA levels. The first five bars represent mean fold change in total 22GRNAs normalized to odor-insensitive sn2343 RNA in adapted versus naive animals of the indicated genotype. Error bars represent SEM. Red line indicates no change. * = $p < 0.03$,

(legend continued on next page)

(Hedgecock et al., 1990; Colon-Ramos et al., 2007). The gene structure, along with the amplicons derived from mRNA, 22GRNA, and genomic DNA, are indicated in Figure 2A.

Nuclear RNAi silences gene expression, leading to lower levels of target mRNA. To determine whether *odr-1* message levels are decreased in odor-adapted populations, we performed quantitative real-time PCR on RNA collected from the same samples that showed behavioral adaptation to butanone (Figure S2A). We found that *odr-1* mRNA decreased by approximately one half in odor-adapted as compared to naive populations (Figure 2B, second bar). By comparison, *unc-40* mRNA levels were unchanged (Figure 2B, first bar). In *mut-7(pk204)* animals, *odr-1* mRNA levels were not odor responsive (Figure 2B, third bar, Figure S2A for individual assays and behavior), but expression of MUT-7 solely within AWC partially restored odor responsiveness (Figure 2B, fourth bar). Thus, in odor-adapted populations, the *odr-1* mRNA decreases, and these changes depend on odor exposure as well as functional MUT-7.

To understand whether the modest decrease in *odr-1* mRNA (Figure 2B) has a behavioral consequence, we asked whether the level of *odr-1* mRNA correlates with the CI of odor-adapted populations. We found that the levels of *odr-1* mRNA correlated strongly with odor attractiveness (Figure 2C). The correlation between CI and *odr-1* mRNA was even stronger in the *mut-7(pk204)* strains that expressed MUT-7 solely in the AWC neuron (Figure 2C). This indicates that the decreases we observe in *odr-1* mRNA in AWC could be responsible for the stably diminished odor attractiveness that is the hallmark of long-term adaptation.

In the analysis described above, we examined mRNA from whole worms, but two lines of evidence indicate that this drop in mRNA occurs within the AWC neurons: loss of *odr-1* leads to the adapted phenotype, and this is rescued by expression of ODR-1 in the AWC neurons (L'Etoile and Bargmann, 2000), and overexpression of ODR-1 in AWC alone blocks adaptation (L'Etoile and Bargmann, 2000). Taken together, the data implicate downregulation of the *odr-1* gene in AWC in butanone adaptation.

odr-1-Directed 22GRNA Increases in the AWC Sensory Neuron of Adapted Animals

To determine whether there is evidence for the endo-RNAi pathway acting in adaptation, we used quantitative real-time PCR to compare the levels of *odr-1* and *unc-40* 22GRNA species in naive and butanone-adapted populations. We found that expression of the *odr-1* 22GRNA odr-1.7 increased by more than 2-fold in adapted animals compared to naive controls (Figure 2D, second bar, and Figure S2B). The levels of a less abundant 22GRNA, odr-1.6, and unc-40.2, however, did not change significantly (red line indicates a ratio of 1:1 for adapted to naive levels) (Figure 2D, first and third bars, and Figure S2B). Thus, a 22GRNA (odr-1.7) complementary to the *odr-1* gene increases in animals adapted to odor.

These measurements of 22GRNAs reflect levels throughout the animal, including the germline (Gu et al., 2009). To determine whether odr-1.7 22GRNA is regulated by odor specifically in AWC, we analyzed 22GRNA from animals that expressed MUT-7 only in AWC (Figure 1D). Though total odr-1.7 22GRNA levels were insensitive to odor exposure in *mut-7*-defective animals, expression of MUT-7 in AWC restored odor responsiveness to this species of 22GRNA (Figure 2D, fourth and fifth bars, and Figure S2B). Thus, the levels of odr-1.7 22GRNA are increased by odor exposure when a factor required for 22GRNA accumulation (Gu et al., 2009) is expressed solely within the AWC neuron.

odr-1 siRNAs Are Loaded onto NRDE-3 in Adaptation

To better understand how the nuclear RNAi pathway might function in odor adaptation, we asked whether odr-1.7 or unc-40.2 22GRNAs associate with NRDE-3. We probed this association by IPing 3XFLAG-tagged NRDE-3 (see Figure S2C for behavior). We found odr-1.6, 1.7 and unc-40.2 coimmunoprecipitated with NRDE-3. The level of odr-1.7 22GRNA in association with NRDE-3 was increased significantly in adapted animals (Figure 2D, seventh bar). By contrast, levels of coimmunoprecipitated odr-1.6 or unc-40.2 22GRNA were not changed in the same animals, indicating that NRDE-3 specifically binds more odr-1.7 22GRNA in adapted animals. This finding supports a model in which ODR-1 mRNA is reduced by NRDE-3/odr-1.7 22GRNA, mediating downregulation of the *odr-1* gene.

HPL-2 Associates with the *odr-1* Locus in Odor-Adapted AWC Neurons

One biochemical readout of siRNA/NRDE-3-directed silencing is increased heterochromatin deposition at the targeted locus (Burkhart et al., 2011; Guang et al., 2010; Gu et al., 2012). To understand whether odr-1.7/NRDE-3 might target the *odr-1* locus in the odor-adapted AWC neuron, we expressed 3XFLAG-tagged heterochromatin associated factor, HPL-2, from the *odr-3* promoter (which drives expression in AWCs and four other neurons; see Figure S2D for behavior). When we performed chromatin immunoprecipitation (ChIP) of HPL-2 followed by qPCR on naive and behaviorally adapted populations, we found that ChIP of the *odr-1* locus was increased in adapted AWC neurons (Figure 2E). The greatest increase in HPL-2-associated

Wilcoxon signed-rank test for median values versus no change. p values displayed are the comparison of medians using an unpaired two sample Mann Whitney nonparametric t test, n > 3. Figure S2B is associated with this panel. The last three bars represent mean fold change in p*nrde-3*::NRDE-3 coIPed 22GRNA (n = 6) normalized to the odor-insensitive X-cluster. Error bars represent SEM. * = p < 0.04, Wilcoxon signed rank test for median values versus no change. Displayed p values are from a pairwise, one-tailed t test, p = 0.0469 of medians. Figure S2C shows the behavior.

(E) Prolonged odor exposure specifically increases HPL-2 binding to the *odr-1* locus in a MUT-7-dependent fashion. The mean ratio of 3XFLAG-HPL-2 expressed in AWC (p*odr-3*) coimmunoprecipitated *odr-1* (dark bars) or *unc-40* (light bars) in adapted versus naive animals is shown above the genotype of each population. Error bars represent SEM. Also indicated is the PCR-amplified, coIPed region of each locus corresponding to "A," "B," and "C" in (A). Coimmunoprecipitated DNA from each locus was normalized to input. This was then normalized to the ratio of IPed *act-3* to input. *act-3* levels were odor insensitive. *p = 0.031, one-tailed Wilcoxon signed-rank test comparing median values to no change (the red line). The median value of *odr-1* B was compared to *unc-40* B; p = 0.0079 using a two-tailed Mann Whitney test. n = 5. The final set of bars represents background from nontransgenic animals. Figure S2D shows the behavior.

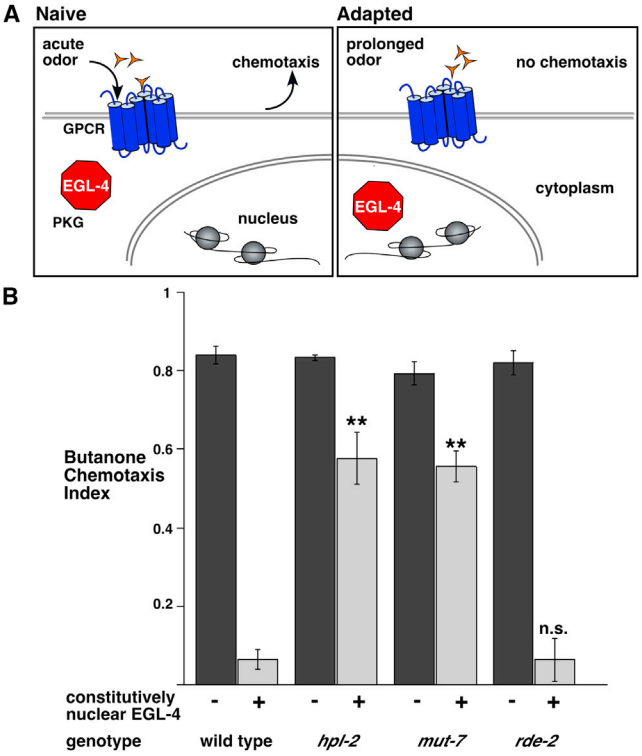

C

genotype	% population with nuclear EGL-4 in AWC	
	naive	butanone exposed
wild type	12 (n=68)	99 (n=99)
hpl-2	12 (n=86)	89 (n=114)
mut-7	5 (n=88)	89 (n=93)

Figure 3. HPL-2 and MUT-7 Act Downstream of Nuclear EGL-4

(A) Current model for long-term olfactory adaptation of the AWC neuron. Acute stimulation of AWC localized G-protein-coupled receptors (GPCR) by odor (left) causes animals to chemotax toward the odor. After prolonged odor exposure (right), the cGMP-dependent protein kinase (PKG) EGL-4 translocates to the nucleus to cause animals to ignore the odor for prolonged periods of time.

(B) Once in the nucleus, EGL-4 requires HPL-2 and MUT-7 to promote adaptation. The chemotaxis index of the indicated strains that express constitutively nuclear EGL-4 from a transgene (+) were compared to their siblings that did not carry this transgene (−). *rde-2* is a control, adaptation-proficient strain (Figure S1A). Importantly, all animals were naive to butanone. $n > 3$ with >100 animals analyzed per assay. $^{**}p < 0.0001$, two-tailed Student's t test. Bars represent the mean CIs, and the error bars represent SEM.

(C) HPL-2 and MUT-7 are not required for odor-induced nuclear entry of EGL-4. GFP-tagged EGL-4 was expressed in either wild-type, *hpl-2(tm1489)*, or *mut-7(pk204)* strains. Animals were exposed to buffer alone (naive) or butanone for 80 min before imaging. The percentage of the population that showed nuclear EGL-4 in one AWC neuron was determined.

ChIP (8-fold higher in adapted than in naive) was located just downstream of the region encoding odr-1.7. Further, the odor-dependent increase was not seen at the *unc-40* locus. As a specificity control for the 22GRNA pathway, we performed ChIP from *mut-7* loss-of-function animals, which show no increase in odr-1.7 22GRNA levels in response to odor and likewise show no increase in *odr-1* ChIP (Figure 2E). These results show that *odr-1* is a target for increased HPL-2 association in the odor-adapted AWC. Though this is not the only interpretation, these results are most consistent with nuclear RNAi targeting this locus.

HPL-2 Is a Direct Phosphorylation Target of the Odor-Responsive Kinase, EGL-4

How might an environmental signal such as odor intersect with the endogenous nuclear RNAi pathway to mediate adaptation? Prolonged odor stimulation causes nuclear accumulation of the cGMP-dependent protein kinase EGL-4 (Figure 3A) (O'Halloran et al., 2009; Lee et al., 2010), and nuclear EGL-4 is both necessary and sufficient to induce long-term odor adaptation. Indeed, expression of constitutively nuclear EGL-4 (NLS-EGL-4) in AWC decreased chemotaxis toward inherently attractive odors even in naive animals (Figure 3B) (Lee et al., 2010; O'Halloran et al., 2009). MUT-7 or HPL-2 could thus act by promoting nuclear accumulation of EGL-4. However, we found that nuclear accumulation of EGL-4 was not altered in *mut-7* or *hpl-2* mutant strains (Figure 3C). Three lines of evidence led us to hypothesize instead that EGL-4 promotes adaptation by phosphorylating and activating MUT-7 and HPL-2. First, we found that constitutively nuclear EGL-4 required both HPL-2 and MUT-7 to induce adaptation in naive animals (Figure 3B). Second, predicted EGL-4 phosphorylation sites within MUT-7 and HPL-2 (Figure 4A) are required for adaptation (Figures 4B, 4C, and S3). Third, expression of phospho-defective MUT-7 in wild-type animals caused adaptation defects, suggesting that MUT-7 phosphorylation is required for this behavioral change (Figure S3D).

MUT-7 and HPL-2 might be direct targets of the EGL-4 kinase; thus, we asked whether NLS-EGL-4 phosphorylates these factors in vitro. We were unable to purify full-length MUT-7, so we focused on HPL-2. We found that *C. elegans* expressed immunopurified NLS-EGL-4 phosphorylated recombinant HPL-2 and that the level of ^{32}P incorporation diminished when the predicted PKG phosphorylation sites within HPL-2 were mutated (Figures 4D and S3G). We therefore conclude that these sites are direct targets of EGL-4 in vitro. Thus, it is likely that HPL-2, a nuclear protein, is directly phosphorylated by EGL-4 once it enters the AWC nucleus.

Phosphorylation of HPL-2 at EGL-4 Target Sites Is Both Necessary and Sufficient to Promote Odor Adaptation

If nuclear EGL-4 promotes odor adaptation by phosphorylating HPL-2 or MUT-7, then mimicking phosphorylation at consensus sites is predicted to promote adaptation in naive animals. To test this, we replaced the serines and threonines at each predicted EGL-4 phosphorylation site in MUT-7 and each in vitro verified site in HPL-2 with the phosphomimetic, glutamic acid (Mansour et al., 1994). Expression of the phosphomimetic form of MUT-7 in wild-type worms had no effect on chemotaxis. Because only ~50% of known functions of phosphorylated residues can be mimicked by glutamic acid substitutions (Maciejewski et al., 1995), we can make no conclusions about MUT-7 phosphorylation. However, expressing the phosphomimetic form of HPL-2 in wild-type animals substantially reduced naive attraction to butanone, whereas expression of the wild-type HPL-2 had no effect (Figure 4E). Thus, mimicking phosphorylation of HPL-2 at EGL-4 target residues is sufficient to

promote behavior that resembles the adapted state. When each site was analyzed individually, we found that HPL-2(S155E), which lies in the chromo shadow domain (CSD), had the greatest effect (Figure S3E).

HPL-2 (all S/T to E) could act as a gain-of-function mutation that engages the adaptation machinery in the absence of odor, or it could nonspecifically diminish AWC function. To distinguish between these possibilities, we expressed HPL-2 (all S/T to E) in mutants that lack the downstream adaptation-promoting factor, OSM-9 (Colbert and Bargmann, 1995). These animals were able to chemotax significantly better to butanone than the parental strain (Figure 4F). Thus HPL-2(all S/T to E) promotes adaptation upstream of OSM-9. We conclude that phosphorylation of HPL-2 at EGL-4 target sites is sufficient to promote adaptation even in the absence of odor exposure. Importantly, EGL-4 is the only PKG in *C. elegans* that is required for odor adaptation (Figure S3H). Thus, it is likely that odor acts via EGL-4 to activate HPL-2.

To understand whether the siRNA pathway was required for HPL-2(all S/T to E) to induce adaptation, we asked whether *mut-7* was required for this gain-of-function phenotype. Loss-of-function MUT-7 (*mut-7(pk204)*) suppressed the ectopic adaptation seen in naive animals expressing HPL-2(all S/T to E) (Figure 4F). Thus, phosphorylation of HPL-2 is both necessary and sufficient for adaptation, but it requires fully functional MUT-7. This is consistent with the ChIP studies in Figure 2E that show that accumulation of HPL-2 at the *odr-1* locus of adapted worms requires functional MUT-7. The observation that HPL-2(allS/T to E) promotes adaptation in the naive animal—and yet loss of MUT-7 blocks this adaptation—indicates that, in the naive animal, there is sufficient MUT-7-dependent RNAi to engage the adaptation process.

DISCUSSION

An emerging paradigm is that small noncoding RNAs provide memory of nonself gene expression (Shirayama et al., 2012); this work extends the role of siRNAs to encoding memory of the environment and experience. We provided evidence that, in the olfactory sensory neurons (AWCs) of adult-behaving *C. elegans*, endogenous RNAi promotes odor adaptation by repressing the *odr-1* gene (Figure 5). Our data show that, in response to prolonged odor exposure, *odr-1*-directed 22GRNAs increase, and this increase is most likely to occur in the AWC neuron (Figure 2D). We demonstrated that these 22GRNAs are loaded on to the nuclear Ago, NRDE-3 (Figure 2D), that acts in AWC (Figure 1G). NRDE-3 may shuttle the *odr-1* 22GRNA into the AWC nucleus, and we have direct evidence that the HP1 homolog, HPL-2, is loaded on to the *odr-1* gene in response to odor (Figure 2E). We provide in vitro evidence that HPL-2 can be phosphorylated by nuclear EGL-4 (Figure 4). Mimicking phosphorylation of HPL-2 is sufficient to evoke adaptation behavior. Phosphorylation of HPL-2 would repress the *odr-1* gene and ultimately lead to the reduced levels of *odr-1* mRNA seen in adapted animals (Figure 2B). This reduction in *odr-1* mRNA correlates strongly with behavior (Figure 2C). One gap in this model is that we do not know whether NRDE-3 or *odr-1* 22GRNA bind the *odr-1* locus. An alternate explanation is that *odr-1* is repressed by a factor that is itself negatively regulated by a second factor that is repressed by NRDE-3 and the RNAi pathway. In this scheme, the repressive factor that binds to the *odr-1* regulatory regions would set up repressive chromatin marks that center at the same part of the *odr-1* gene that encodes the *odr-1* 22GRNA bound by NRDE-3. However, the proposed model is more parsimonious and consistent with the data than the alternative model and leads to the exciting hypothesis that RNAi may act broadly as a biological rheostat to allow stimulation to dampen gene expression and may promote cells to alter their responses as a function of previous stimulation.

Specificity of Odor Adaptation within AWC Neurons

Butanone adaptation does not affect attraction to benzaldehyde or isoamyl alcohol (Colbert and Bargmann, 1995), so how would downregulation of ODR-1, a GC required for all AWC responses (L'Etoile and Bargmann, 2000), specifically adapt the butanone response? The other odors are sensed by both left and right AWCs, and butanone is sensed by only one AWC (Wes and Bargmann, 2001). Indeed, prolonged butanone exposure results in nuclear EGL-4 in only one AWC (Lee et al., 2010). Thus, reducing the levels of ODR-1 in the butanone responsive neuron should not affect chemotaxis mediated by the other AWC. Furthermore, each odor requires different factors for adaptation (Colbert and Bargmann, 1995), and thus, each response may have unique sensitivity to the level of ODR-1.

The Nuclear RNAi Pathway Acts with HP1 in Odor Adaptation

We found that the nuclear Argonaute NRDE-3 is required in AWC for odor adaptation, and it binds *odr-1* siRNA in an odor-dependent fashion. Prior work showed that NRDE-3 acts in the nucleus along with NRDE-2, NRDE-1, and NRDE-4 to establish H3K9me3 marks on the target locus, thereby silencing transcription (Burkhart et al., 2011; Burton et al., 2011; Gu et al., 2012; Guang et al., 2010). This connection between endo-siRNA, H3K9me3 marks, and gene silencing was originally reported in *S. pombe*, in which silencing involves deposition of H3K9me3 marks directed by siRNAs produced from pericentromeric repeat regions and the mating type locus (Aygün and Grewal, 2010). In *pombe*, these siRNAs induce a transcriptional silencing complex (RITS) that localizes chromatin to specific nascent transcripts. A feed-forward silencing loop is established as chromodomain proteins, including the HP1 homolog, and methyltransferases are nucleated by RITS complexes and in turn recruit more methyltransferases. Concurrently, RNA-dependent RNA polymerase complexes (RDRCs) are recruited, thus increasing siRNA production (Hayashi et al., 2012; Rougemaille et al., 2012; Yamanaka et al., 2013). A direct link between chromatin, RNAi, and RITS was demonstrated when the CSD of *pombe* HP1 was shown to interact with several members of the RNAi and RITS machinery via the HP1-binding protein, Ers1 (Rougemaille et al., 2012). Because Ers1 interacted specifically with the CSD of yeast HP1, and we show that in *C. elegans*, phosphorylation of this domain is sufficient to induce adaptation, we speculate that the *C. elegans* HPL-2 CSD likewise nucleates RNAi factors on genes such as *odr-1* whose silencing promotes adaptation. Indeed, because loss of *mut-7* suppressed the gain-of-function HPL-2(S155E), MUT-7 may either act along with or

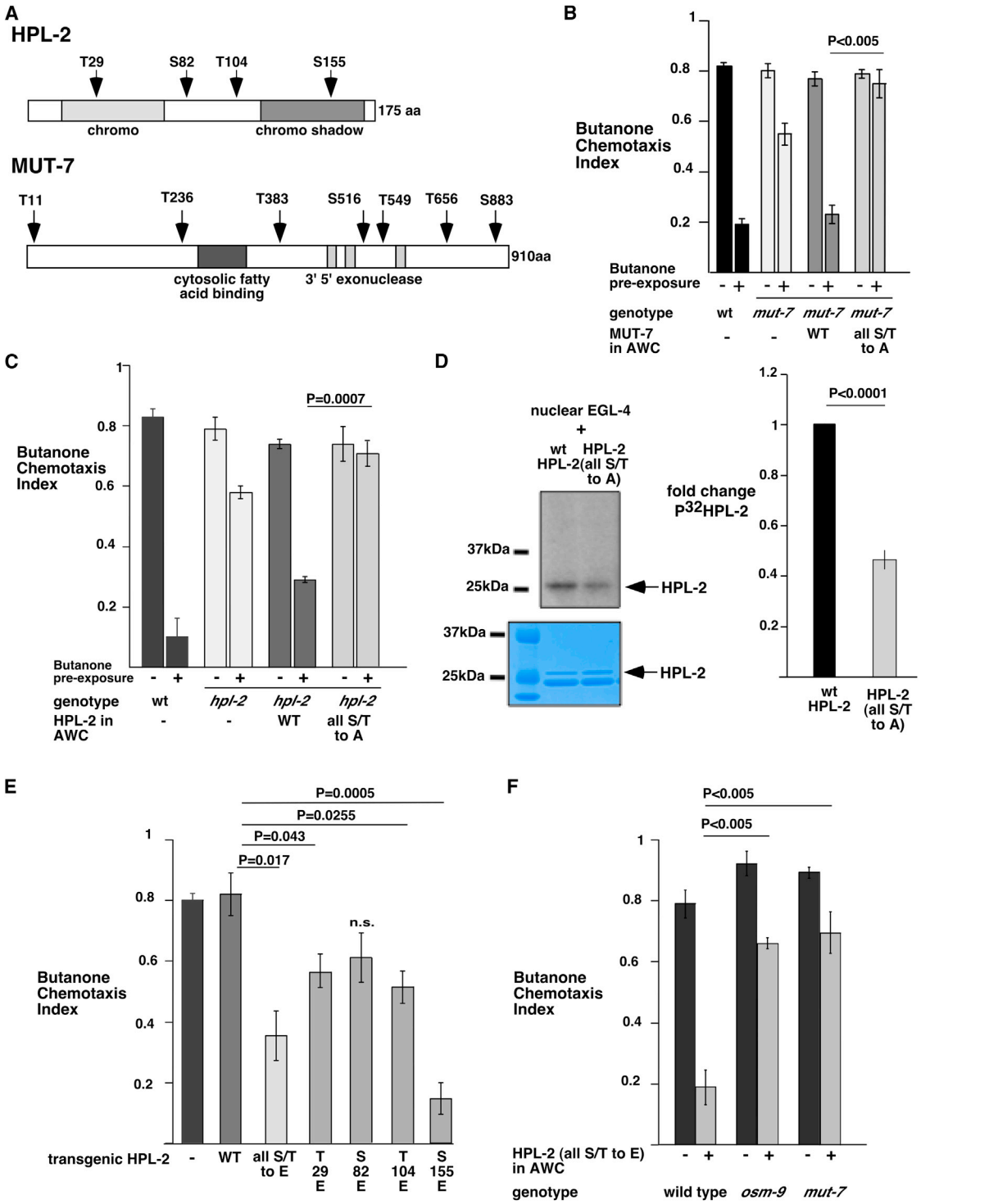

Figure 4. Phosphorylation of HPL-2 and MUT-7 at Predicted PKG Sites Is Required for Adaptation

(A) Schematic of HPL-2 and MUT-7. (Top) HPL-2 contains an N-terminal chromodomain, a C-terminal chromo shadow domain, and four predicted PKG phosphorylation sites. (Bottom) MUT-7 contains two predicted functional domains—cytosolic fatty acid binding domain and 3′ to 5′ exonuclease—and seven predicted PKG phosphorylation sites.

(B) Phosphorylation of predicted PKG target sites in MUT-7 is required for adaptation. Mean CIs of wild-type or *mut-7(pk204)* strains expressing the indicated form of MUT-7 in AWC. Figure S3D shows individual lines. n = 3 and p value is from a two-tailed Student's t test. The lines rescued the sterility defects of *mut-7(pk204)* (Figure S3B).

(legend continued on next page)

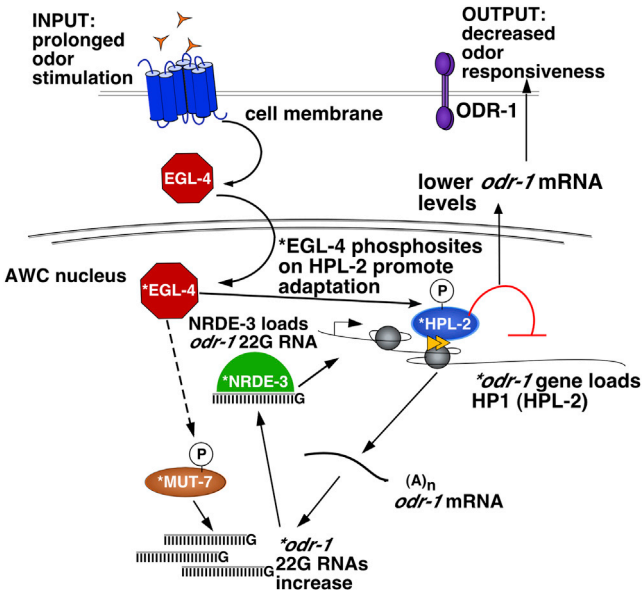

Figure 5. Prolonged Stimulation Induces Long-Term Olfactory Adaptation in the AWC Neurons via an siRNA and Chromatin-Remodeling-Dependent Process

Model for how prolonged butanone stimulation may lead to long-lasting olfactory adaptation in the AWC neuron. Asterisks indicate processes and factors shown to act in AWC. Odor exposure stimulates a seven transmembrane GPCR at the cell membrane and causes EGL-4 to enter the nucleus where it phosphorylates HPL-2 (solid arrow) and may also phosphorylate MUT-7 (dashed arrow). Phosphorylated HPL-2 promotes adaptation in a 22GRNA dependent process by binding to H3K9me3 (yellow flags). Phosphorylated MUT-7 boosts levels of *odr-1* 22G RNAs. These siRNAs act as guides within the NRDE-3 Ago complex to direct H3K9me3 to *odr-1* gene. Phosphorylated HPL-2 would repress transcription of the *odr-1* gene (red inhibitory bar). Finally, lower levels of *odr-1* mRNA decreases the animal's attraction to butanone.

downstream of activated HPL-2. Thus, our data are consistent with HPL-2 being recruited to siRNA-targeted loci by H3K9me3 marks and perhaps also nucleating an RNAi-based feed-forward loop in an analogous fashion to its role in *S. pombe*.

Chromatin Marks in Behavior

HPL-2 loads onto the *odr-1* locus in odor-adapted AWCs. This may reflect deposition of a heterochromatic mark. Such marks have been implicated in both neuronal development, as well as in stimulus-induced changes in behavior. H3K9me3-mediated silencing of all but the active olfactory receptor allows for monoallelic expression of odor receptors in the mammalian nasal epithelium (Magklara et al., 2011). In rodents, behavioral addiction to cocaine has been shown to increase H3K9me2 marks within a key brain reward region (Renthal et al., 2009), and regulation of H3K9 methylation is important for addiction-induced neuroplasticity (Maze et al., 2010). These studies highlight the importance of histone methylation marks in regulating long-term behavioral states and may indicate that recruitment of these marks to specific locations could be a key regulated process. It remains to be seen whether such marks can be directed to genes via the action of endo-siRNAs.

Evidence that mammals have a dicer-dependent class of 22GRNAs is currently lacking (Babiarz et al., 2011). In *S. pombe*, however, siRNA species derived from protein-coding genes were not identified until nuclear exosome deficient cells were used (Yamanaka et al., 2013). Such degradation processes might also conceal endo-siRNAs in higher eukaryotes. Though no RNA-dependent RNA polymerase has yet been identified in mammals, it is possible that other classes of small RNAs such as mitrons (miRNAs processed from introns) play an analogous function in the mammalian brain or that RNA polymerase I, II, or III might be recruited to produce small antisense RNAs (Filipovska and Konarska, 2000; Lehmann et al., 2007; Greco-Stewart et al., 2009). These RNAs could similarly direct deposition of chromatin marks and affect behavior.

Odor Regulates Chromatin Changes

Our work indicates that an environmental signal is likely to act via a kinase to amplify the small RNA-directed process. Kinases have been widely appreciated to effect behavioral responses: mitogen-activated protein kinases, calcium calmodulin-dependent protein kinase II, protein kinase C, and protein kinase A can each contribute to the formation of long-term memory subsequent to repeated training (Dash et al., 2007; Gerstner et al., 2009). Indeed, EGL-4 acts via a histone deacetylase (HDA class I) in the nucleus of uterine epithelium cells to promote egg laying (Hao et al., 2011). Here, we demonstrate that the HP1 homolog, HPL-2, is a direct target of this odor-dependent kinase.

In both yeast and mammals, HP1 phosphorylation has been shown to regulate HP1's repressive activity in response to inter- and intracellular signals. Although many studies highlighted the important role played by modifications of the CD (Shimada and Murakami, 2010), our observations suggest that modifications of the CSD may be equally important. The CSD serves as a

(C) Phosphorylation of HPL-2 at predicted PKG sites is required for adaptation. CIs of animals of the indicated genotype that expressed the indicated form of HPL-2 cDNA in AWC are shown. n > 3 with >100 individuals per assay. p value is from an unpaired Student's t test.

(D) Nuclear EGL-4 phosphorylates HPL-2 in vitro. (Left) 3XFLAG-nuclear EGL-4 kinase was immunopurified from worms (behavior in Figure S3F) and incubated with purified HPL-2 and ^{32}P ATP. The reactions were resolved on a gel and stained with Coomassie blue as loading control (lower) followed by autoradiography (upper). (Right) Quantification of five independent kinase assays. ^{32}P phosphorylated HPL-2 was normalized to Coomassie stained band. Values shown for mutant HPL-2 substrate are shown as fold reduction of phosphorylation relative to HPL2-wild-type, which was set to 1. Error bars represent mean ± SEM ($p < 0.0001$; two-tailed Student's t test, n = 5).

(E) Phosphorylation of HPL-2 at a predicted PKG phosphorylation site in the CSD is sufficient to decrease butanone chemotaxis in naive animals. CIs of wild-type animals expressing the indicated form of HPL-2 in AWC, n > 3. Figure S3E shows CIs of individual lines. All strains expressed similar levels of the indicated transgenes as assessed by GFP intensity. p values are from a two-tailed Student's t test.

(F) Phosphorylation of HPL-2 at the EGL-4 phosphorylated sites is sufficient to promote adaptation in naive animals. CIs of naive wild-type, *osm-9*, or *mut-7* animals either expressing the phosphomemetic HPL-2(S/Tto E) (+) or not (–). In all panels of this figure, the bars represent the mean values, and the error bars represent SEM; n > 5. p value is from an unpaired two-tailed Student's t test.

platform for the assembly of other chromatin (Couteau et al., 2002) and RNAi (Rougemaille et al., 2012) -associated proteins and may therefore represent an attractive target for dynamic regulation of transcriptional states. The CSD is required for HP1 homodimerization and formation of an interaction platform with proteins containing the PxVxL interaction motif (Cowieson et al., 2000; Thiru et al., 2004). Though basal silencing requires phosphorylation of the CSD (Zhao et al., 2001), our data indicate that CSD phosphorylation may also be used for signal responsive silencing in neurons.

Other kinases may act in a similar fashion to EGL-4 in other cells and organisms to allow developmental or environmental signals to enhance small-RNA-dependent gene silencing. By regulating RITS, all siRNA-producing loci could be coordinately silenced at a point in time, and the ensuing chromatin changes would ensure stable silencing. Such widespread silencing by siRNAs may allow experiences to alter expression of whole cohorts of genes in the context of both development and behavior.

EXPERIMENTAL PROCEDURES

Worm Strains

For a complete list of strains used, please see the Supplemental Information. Bristol N2 was the wild-type strain.

Plasmid Construction and Transgenic Strains

Details of plasmid construction can be found in the Supplemental Information.

Behavior

Behavioral assays were conducted on day one adults as described (Colbert and Bargmann, 1995). More details are presented in the Supplemental Information. For heat shock experiments, worms on their original growth plates were exposed to 30°C for 1 hr and then recovered at 20°C for 2 hr prior to behavioral assays.

Kinase Assay with Nuclear EGL-4

To evaluate nuclear NLS FLAG-EGL-4 kinase activity, 100 μg of worm lysate was immunoprecipitated using anti-FLAG M2 magnetic beads (Sigma-Aldrich). Bead-bound immunoprecipitates were washed extensively with kinase buffer. Then kinase assays were performed directly on the beads by adding 1.5 μg of substrate (HPL-2 WT, HPL-2[all S/T-A], or Histone H1), 2 μCi ^{32}P ATP (PerkinElmer), and 25 μM cGMP (Sigma-Aldrich).

Details are in the Supplemental Information.

Isolation of NRDE-3-Associated Small RNA

50–60 plates of adult animals expressing 3XFLAG::GFP::NRDE-3 were collected, and half the population was incubated with SBasal alone, and the other half was incubated with SBasal plus butanone for 80 min. Behavior of ~100 animals from each was assessed. Extracts were made from the remaining animals as described (Guang et al., 2008 and Supplemental Information).

Isolation of HPL-2-Associated DNA

p*odr-3*::3XFLAG::GFP::HPL-2 was integrated into the genome and outcrossed five times. 100 plates of adult animals were harvested, and half were exposed to buffer and half to butanone and buffer. ~100 animals from each were assayed. The remaining animals were processed for ChIP (Gerstein et al., 2010). Only populations that showed an adapted CI of 0.05–0.3 were used. Details of the ChIP are in the Supplemental Information. Quantitation of coimmunoprecipitated DNA is described in the Supplemental Information.

Quantitative Real-Time PCR

For RNA analysis, 5 plates of day one adult animals were collected and treated to the adaptation protocol, and their behavior was assessed. Total RNA was isolated as described in the Supplemental Information. Total RNA from entire worms was used in 22GRNA and mRNA quantitation as described in Supplemental Information.

To quantify HPL-2-associated DNA, ChIP results were analyzed by qPCR using Brilliant III Ultra-Fast SYBR Green qPCR Master Mix (Agilent Technologies).

The primers were specific to the *odr-1*, *unc-40*, or *act-3* loci. The levels of the housekeeping gene *act-3* did not change with odor. Please see Extended Experimental Procedures and Table S2 for details and primers.

SUPPLEMENTAL INFORMATION

Supplemental Information includes Extended Experimental Procedures, three figures, and two tables and can be found with this article online at http://dx.doi.org/10.1016/j.cell.2013.08.006.

ACKNOWLEDGMENTS

We thank Maria Gallegos, Mehrdad Matloubian, Bassem Al-Sady, Jonathan Isaiah Gent, Georgia Woods, and Robert Blelloch; members of the L'Etoile lab: Damien O'Halloran, Scott Hamilton, Sarah Gerhart, Mary Bethke, and Chantal Brueggemann; and members of the Kennedy lab: Bethany Buckley and Kirk Burkhart, for critical reading and helpful discussions. We thank Shi-Yu Chen for purified MUT-7 and HPL-2. We thank Ahmed Elewa and Craig Mello for good discussions, worm strains, and *odr-1* 22G RNA sequences; Ebenezer Yamoah for use of his qPCR system; and Kohta Ikegami and Susan Strome for ChIP protocols and advice. We also thank Nadia Gronachon, Kim Collins, Christopher Morales, Anu Gupta, and Aarati Asundi for help with worm culture; Bethany Buckley, the Caenorhabditis Genetics Center and the National Bioresource Project for numerous strains, and Yuji Kohara for yk cDNA clones. We thank Leah Frater (Anderson lab), Derek Pavelec (Kennedy lab), Jay Maniar, and Jonathan Gent (Fire lab) for producing and sharing unpublished sequencing reads. N.D.L. acknowledges support from NSF 0954258 and NIH R01DC005991. B.-T.J. conceived of and carried out experiments and cowrote the manuscript. L.S. developed, optimized, and performed kinase assays. CG performed RNA and DNA analysis. L.S. and C.G. contributed equally to the manuscript. A.G., F.P., and S.K. provided unpublished protocols, reagents, support and insight. N.L. analyzed data and wrote the manuscript.

Received: April 7, 2013
Revised: July 16, 2013
Accepted: August 1, 2013
Published: August 29, 2013

REFERENCES

Aoki, K., Moriguchi, H., Yoshioka, T., Okawa, K., and Tabara, H. (2007). In vitro analyses of the production and activity of secondary small interfering RNAs in C. elegans. EMBO J. *26*, 5007–5019.

Ashe, A., Sapetschnig, A., Weick, E.M., Mitchell, J., Bagijn, M.P., Cording, A.C., Doebley, A.L., Goldstein, L.D., Lehrbach, N.J., Le Pen, J., et al. (2012). piRNAs can trigger a multigenerational epigenetic memory in the germline of C. elegans. Cell *150*, 88–99.

Aygün, O., and Grewal, S.I. (2010). Assembly and functions of heterochromatin in the fission yeast genome. Cold Spring Harb. Symp. Quant. Biol. *75*, 259–267.

Babiarz, J.E., Hsu, R., Melton, C., Thomas, M., Ullian, E.M., and Blelloch, R. (2011). A role for noncanonical microRNAs in the mammalian brain revealed by phenotypic differences in Dgcr8 versus Dicer1 knockouts and small RNA sequencing. RNA *17*, 1489–1501.

Bargmann, C.I., Hartwieg, E., and Horvitz, H.R. (1993). Odorant-selective genes and neurons mediate olfaction in C. elegans. Cell *74*, 515–527.

Black, J.C., and Whetstine, J.R. (2011). Chromatin landscape: methylation beyond transcription. Epigenetics *6*, 9–15.

Buckley, B.A., Burkhart, K.B., Gu, S.G., Spracklin, G., Kershner, A., Fritz, H., Kimble, J., Fire, A., and Kennedy, S. (2012). A nuclear Argonaute promotes multigenerational epigenetic inheritance and germline immortality. Nature *489*, 447–451.

Burkhart, K.B., Guang, S., Buckley, B.A., Wong, L., Bochner, A.F., and Kennedy, S. (2011). A pre-mRNA-associating factor links endogenous siRNAs to chromatin regulation. PLoS Genet. *7*, e1002249.

Burton, N.O., Burkhart, K.B., and Kennedy, S. (2011). Nuclear RNAi maintains heritable gene silencing in Caenorhabditis elegans. Proc. Natl. Acad. Sci. USA *108*, 19683–19688. http://dx.doi.org/10.1073/pnas.1113310108.

Claycomb, J.M., Batista, P.J., Pang, K.M., Gu, W., Vasale, J.J., van Wolfswinkel, J.C., Chaves, D.A., Shirayama, M., Mitani, S., Ketting, R.F., et al. (2009). The Argonaute CSR-1 and its 22G-RNA cofactors are required for holocentric chromosome segregation. Cell *139*, 123–134.

Colbert, H.A., and Bargmann, C.I. (1995). Odorant-specific adaptation pathways generate olfactory plasticity in C. elegans. Neuron *14*, 803–812.

Colbert, H.A., and Bargmann, C.I. (1997). Environmental signals modulate olfactory acuity, discrimination, and memory in Caenorhabditis elegans. Learn. Mem. *4*, 179–191.

Colon-Ramos, D.A., Margeta, M.A., and Shen, K. (2007). Glia promote local synaptogenesis through UNC-6 (netrin) signaling in C. elegans. Science *318*, 103–106.

Coustham, V., Bedet, C., Monier, K., Schott, S., Karali, M., and Palladino, F. (2006). The C. elegans HP1 homologue HPL-2 and the LIN-13 zinc finger protein form a complex implicated in vulval development. Dev. Biol. *297*, 308–322.

Couteau, F., Guerry, F., Muller, F., and Palladino, F. (2002). A heterochromatin protein 1 homologue in Caenorhabditis elegans acts in germline and vulval development. EMBO Rep. *3*, 235–241.

Cowieson, N.P., Partridge, J.F., Allshire, R.C., and McLaughlin, P.J. (2000). Dimerisation of a chromo shadow domain and distinctions from the chromodomain as revealed by structural analysis. Curr. Biol. *10*, 517–525.

Dash, P.K., Moore, A.N., Kobori, N., and Runyan, J.D. (2007). Molecular activity underlying working memory. Learn. Mem. *14*, 554–563.

Denli, A.M., Tops, B.B., Plasterk, R.H., Ketting, R.F., and Hannon, G.J. (2004). Processing of primary microRNAs by the Microprocessor complex. Nature *432*, 231–235.

Dernburg, A.F., Zalevsky, J., Colaiácovo, M.P., and Villeneuve, A.M. (2000). Transgene-mediated cosuppression in the C. elegans germ line. Genes Dev. *14*, 1578–1583.

Duchaine, T.F., Wohlschlegel, J.A., Kennedy, S., Bei, Y., Conte, D., Jr., Pang, K., Brownell, D.R., Harding, S., Mitani, S., Ruvkun, G., et al. (2006). Functional proteomics reveals the biochemical niche of C. elegans DCR-1 in multiple small-RNA-mediated pathways. Cell *124*, 343–354.

Etchberger, J.F., Lorch, A., Sleumer, M.C., Zapf, R., Jones, S.J., Marra, M.A., Holt, R.A., Moerman, D.G., and Hobert, O. (2007). The molecular signature and cis-regulatory architecture of a C. elegans gustatory neuron. Genes Dev. *21*, 1653–1674.

Filipovska, J., and Konarska, M.M. (2000). Specific HDV RNA-templated transcription by pol II in vitro. RNA *6*, 41–54.

Fire, A., Xu, S., Montgomery, M.K., Kostas, S.A., Driver, S.E., and Mello, C.C. (1998). Potent and specific genetic interference by double-stranded RNA in Caenorhabditis elegans. Nature *391*, 806–811.

Gao, J., Wang, W.Y., Mao, Y.W., Gräff, J., Guan, J.S., Pan, L., Mak, G., Kim, D., Su, S.C., and Tsai, L.H. (2010). A novel pathway regulates memory and plasticity via SIRT1 and miR-134. Nature *466*, 1105–1109.

Gent, J.I., Lamm, A., Maniar, J.M., Parameswaran, P., Tao, L., and Fire, A.Z. (2010). Distinct stages of siRNA synthesis in an endogenous RNAi pathway in *C. elegans* soma. Mol Cell *37*, 679–689.

Gerstein, M.B., Lu, Z.J., Van Nostrand, E.L., Cheng, C., Arshinoff, B.I., Liu, T., Yip, K.Y., Robilotto, R., Rechtsteiner, A., Ikegami, K., et al.; modENCODE Consortium. (2010). Integrative analysis of the Caenorhabditis elegans genome by the modENCODE project. Science *330*, 1775–1787.

Gerstner, J.R., Lyons, L.C., Wright, K.P., Jr., Loh, D.H., Rawashdeh, O., Eckel-Mahan, K.L., and Roman, G.W. (2009). Cycling behavior and memory formation. J. Neurosci. *29*, 12824–12830.

Ghildiyal, M., and Zamore, P.D. (2009). Small silencing RNAs: an expanding universe. Nat. Rev. Genet. *10*, 94–108.

Greco-Stewart, V.S., Schissel, E., and Pelchat, M. (2009). The hepatitis delta virus RNA genome interacts with the human RNA polymerases I and III. Virology *386*, 12–15.

Grishok, A., Pasquinelli, A.E., Conte, D., Li, N., Parrish, S., Ha, I., Baillie, D.L., Fire, A., Ruvkun, G., and Mello, C.C. (2001). Genes and mechanisms related to RNA interference regulate expression of the small temporal RNAs that control C. elegans developmental timing. Cell *106*, 23–34.

Grishok, A., Sinskey, J.L., and Sharp, P.A. (2005). Transcriptional silencing of a transgene by RNAi in the soma of C. elegans. Genes Dev. *19*, 683–696.

Gu, W., Shirayama, M., Conte, D., Jr., Vasale, J., Batista, P.J., Claycomb, J.M., Moresco, J.J., Youngman, E.M., Keys, J., Stoltz, M.J., et al. (2009). Distinct argonaute-mediated 22G-RNA pathways direct genome surveillance in the C. elegans germline. Mol. Cell *36*, 231–244.

Gu, S.G., Pak, J., Guang, S., Maniar, J.M., Kennedy, S., and Fire, A. (2012). Amplification of siRNA in Caenorhabditis elegans generates a transgenerational sequence-targeted histone H3 lysine 9 methylation footprint. Nat. Genet. *44*, 157–164.

Guang, S., Bochner, A.F., Pavelec, D.M., Burkhart, K.B., Harding, S., Lachowiec, J., and Kennedy, S. (2008). An Argonaute transports siRNAs from the cytoplasm to the nucleus. Science *321*, 537–541.

Guang, S., Bochner, A.F., Burkhart, K.B., Burton, N., Pavelec, D.M., and Kennedy, S. (2010). Small regulatory RNAs inhibit RNA polymerase II during the elongation phase of transcription. Nature *465*, 1097–1101.

Hao, Y., Xu, N., Box, A.C., Schaefer, L., Kannan, K., Zhang, Y., Florens, L., Seidel, C., Washburn, M.P., Wiegraebe, W., and Mak, H.Y. (2011). Nuclear cGMP-dependent kinase regulates gene expression via activity-dependent recruitment of a conserved histone deacetylase complex. PLoS Genet. *7*, e1002065.

Hayashi, A., Ishida, M., Kawaguchi, R., Urano, T., Murakami, Y., and Nakayama, J. (2012). Heterochromatin protein 1 homologue Swi6 acts in concert with Ers1 to regulate RNAi-directed heterochromatin assembly. Proc. Natl. Acad. Sci. USA *109*, 6159–6164.

Hedgecock, E.M., Culotti, J.G., and Hall, D.H. (1990). The unc-5, unc-6, and unc-40 genes guide circumferential migrations of pioneer axons and mesodermal cells on the epidermis in C. elegans. Neuron *4*, 61–85.

Kaye, J.A., Rose, N.C., Goldsworthy, B., Goga, A., and L'Etoile, N.D. (2009). A 3'UTR pumilio-binding element directs translational activation in olfactory sensory neurons. Neuron *61*, 57–70.

Kennedy, S., Wang, D., and Ruvkun, G. (2004). A conserved siRNA-degrading RNase negatively regulates RNA interference in C. elegans. Nature *427*, 645–649.

Ketting, R.F. (2011). The many faces of RNAi. Dev. Cell *20*, 148–161.

Ketting, R.F., Haverkamp, T.H., van Luenen, H.G., and Plasterk, R.H. (1999). Mut-7 of C. elegans, required for transposon silencing and RNA interference, is a homolog of Werner syndrome helicase and RNaseD. Cell *99*, 133–141.

Knight, S.W., and Bass, B.L. (2001). A role for the RNase III enzyme DCR-1 in RNA interference and germ line development in Caenorhabditis elegans. Science *293*, 2269–2271.

L'Etoile, N.D., and Bargmann, C.I. (2000). Olfaction and odor discrimination are mediated by the C. elegans guanylyl cyclase ODR-1. Neuron *25*, 575–586.

L'Etoile, N.D., Coburn, C.M., Eastham, J., Kistler, A., Gallegos, G., and Bargmann, C.I. (2002). The cyclic GMP-dependent protein kinase EGL-4 regulates olfactory adaptation in C. elegans. Neuron *36*, 1079–1089.

Le Thomas, A., Rogers, A.K., Webster, A., Marinov, G.K., Liao, S.E., Perkins, E.M., Hur, J.K., Aravin, A.A., and Tóth, K.F. (2013). Piwi induces piRNA-guided

transcriptional silencing and establishment of a repressive chromatin state. Genes Dev. *27*, 390–399.

Lee, R.C., Hammell, C.M., and Ambros, V. (2006). Interacting endogenous and exogenous RNAi pathways in Caenorhabditis elegans. RNA *12*, 589–597.

Lee, J.I., O'Halloran, D.M., Eastham-Anderson, J., Juang, B.T., Kaye, J.A., Scott Hamilton, O., Lesch, B., Goga, A., and L'Etoile, N.D. (2010). Nuclear entry of a cGMP-dependent kinase converts transient into long-lasting olfactory adaptation. Proc. Natl. Acad. Sci. USA *107*, 6016–6021.

Lee, H.C., Gu, W., Shirayama, M., Youngman, E., Conte, D., Jr., and Mello, C.C. (2012). C. elegans piRNAs mediate the genome-wide surveillance of germline transcripts. Cell *150*, 78–87.

Lehmann, E., Brueckner, F., and Cramer, P. (2007). Molecular basis of RNA-dependent RNA polymerase II activity. Nature *450*, 445–449.

Maciejewski, P.M., Peterson, F.C., Anderson, P.J., and Brooks, C.L. (1995). Mutation of serine 90 to glutamic acid mimics phosphorylation of bovine prolactin. J. Biol. Chem. *270*, 27661–27665.

Magklara, A., Yen, A., Colquitt, B.M., Clowney, E.J., Allen, W., Markenscoff-Papadimitriou, E., Evans, Z.A., Kheradpour, P., Mountoufaris, G., Carey, C., et al. (2011). An epigenetic signature for monoallelic olfactory receptor expression. Cell *145*, 555–570.

Mansour, S.J., Matten, W.T., Hermann, A.S., Candia, J.M., Rong, S., Fukasawa, K., Vande Woude, G.F., and Ahn, N.G. (1994). Transformation of mammalian cells by constitutively active MAP kinase kinase. Science *265*, 966–970.

Maze, I., Covington, H.E., 3rd, Dietz, D.M., LaPlant, Q., Renthal, W., Russo, S.J., Mechanic, M., Mouzon, E., Neve, R.L., Haggarty, S.J., et al. (2010). Essential role of the histone methyltransferase G9a in cocaine-induced plasticity. Science *327*, 213–216.

McNeill, E., and Van Vactor, D. (2012). MicroRNAs shape the neuronal landscape. Neuron *75*, 363–379.

O'Halloran, D.M., Altshuler-Keylin, S., Lee, J.I., and L'Etoile, N.D. (2009). Regulators of AWC-mediated olfactory plasticity in Caenorhabditis elegans. PLoS Genet. *5*, e1000761.

O'Halloran, D.M., Hamilton, O.S., Lee, J.I., Gallegos, M., and L'Etoile, N.D. (2012). Changes in cGMP levels affect the localization of EGL-4 in AWC in Caenorhabditis elegans. PLoS ONE *7*, e31614.

Pak, J., Maniar, J.M., Mello, C.C., and Fire, A. (2012). Protection from feed-forward amplification in an amplified RNAi mechanism. Cell *151*, 885–899.

Rajasethupathy, P., Antonov, I., Sheridan, R., Frey, S., Sander, C., Tuschl, T., and Kandel, E.R. (2012). A role for neuronal piRNAs in the epigenetic control of memory-related synaptic plasticity. Cell *149*, 693–707.

Renthal, W., Kumar, A., Xiao, G., Wilkinson, M., Covington, H.E., 3rd, Maze, I., Sikder, D., Robison, A.J., LaPlant, Q., Dietz, D.M., et al. (2009). Genome-wide analysis of chromatin regulation by cocaine reveals a role for sirtuins. Neuron *62*, 335–348.

Rougemaille, M., Braun, S., Coyle, S., Dumesic, P.A., Garcia, J.F., Isaac, R.S., Libri, D., Narlikar, G.J., and Madhani, H.D. (2012). Ers1 links HP1 to RNAi. Proc. Natl. Acad. Sci. USA *109*, 11258–11263.

Shimada, A., and Murakami, Y. (2010). Dynamic regulation of heterochromatin function via phosphorylation of HP1-family proteins. Epigenetics *5*, 30–33.

Shirayama, M., Seth, M., Lee, H.C., Gu, W., Ishidate, T., Conte, D., Jr., and Mello, C.C. (2012). piRNAs initiate an epigenetic memory of nonself RNA in the C. elegans germline. Cell *150*, 65–77.

Simmer, F., Tijsterman, M., Parrish, S., Koushika, S.P., Nonet, M.L., Fire, A., Ahringer, J., and Plasterk, R.H. (2002). Loss of the putative RNA-directed RNA polymerase RRF-3 makes C. elegans hypersensitive to RNAi. Curr. Biol. *12*, 1317–1319.

Stringham, E.G., Dixon, D.K., Jones, D., and Candido, E.P. (1992). Temporal and spatial expression patterns of the small heat shock (hsp16) genes in transgenic Caenorhabditis elegans. Mol. Biol. Cell *3*, 221–233.

Tabara, H., Sarkissian, M., Kelly, W.G., Fleenor, J., Grishok, A., Timmons, L., Fire, A., and Mello, C.C. (1999). The rde-1 gene, RNA interference, and transposon silencing in C. elegans. Cell *99*, 123–132.

Tabara, H., Yigit, E., Siomi, H., and Mello, C.C. (2002). The dsRNA binding protein RDE-4 interacts with RDE-1, DCR-1, and a DExH-box helicase to direct RNAi in C. elegans. Cell *109*, 861–871.

Thiru, A., Nietlispach, D., Mott, H.R., Okuwaki, M., Lyon, D., Nielsen, P.R., Hirshberg, M., Verreault, A., Murzina, N.V., and Laue, E.D. (2004). Structural basis of HP1/PXVXL motif peptide interactions and HP1 localisation to heterochromatin. EMBO J. *23*, 489–499.

Tops, B.B., Tabara, H., Sijen, T., Simmer, F., Mello, C.C., Plasterk, R.H., and Ketting, R.F. (2005). RDE-2 interacts with MUT-7 to mediate RNA interference in Caenorhabditis elegans. Nucleic Acids Res. *33*, 347–355.

Vasquez-Rifo, A., Jannot, G., Armisen, J., Labouesse, M., Bukhari, S.I.A., Rondeau, E.L., Miska, E.A., and Simard, M.J. (2012). Developmental characterization of the microRNA-specific *C. elegans* Argonautes *alg-1* and *alg-2*. PLoS ONE *7*, e33750. http://dx.doi.org/10.1371/journal.pone.0033750.

Vastenhouw, N.L., Brunschwig, K., Okihara, K.L., Müller, F., Tijsterman, M., and Plasterk, R.H. (2006). Gene expression: long-term gene silencing by RNAi. Nature *442*, 882.

Wes, P.D., and Bargmann, C.I. (2001). C. elegans odour discrimination requires asymmetric diversity in olfactory neurons. Nature *410*, 698–701.

Yamanaka, S., Mehta, S., Reyes-Turcu, F.E., Zhuang, F., Fuchs, R.T., Rong, Y., Robb, G.B., and Grewal, S.I. (2013). RNAi triggered by specialized machinery silences developmental genes and retrotransposons. Nature *493*, 557–560.

Yigit, E., Batista, P.J., Bei, Y., Pang, K.M., Chen, C.C., Tolia, N.H., Joshua-Tor, L., Mitani, S., Simard, M.J., and Mello, C.C. (2006). Analysis of the C. elegans Argonaute family reveals that distinct Argonautes act sequentially during RNAi. Cell *127*, 747–757.

Zhang, C., Montgomery, T.A., Gabel, H.W., Fischer, S.E., Phillips, C.M., Fahlgren, N., Sullivan, C.M., Carrington, J.C., and Ruvkun, G. (2011). mut-16 and other mutator class genes modulate 22G and 26G siRNA pathways in Caenorhabditis elegans. Proc. Natl. Acad. Sci. USA *108*, 1201–1208. http://dx.doi.org/10.1073/pnas.1.

Zhao, T., Heyduk, T., and Eissenberg, J.C. (2001). Phosphorylation site mutations in heterochromatin protein 1 (HP1) reduce or eliminate silencing activity. J. Biol. Chem. *276*, 9512–9518.

EXTENDED EXPERIMENTAL PROCEDURES

Identification of Candidate Adaptation Promoting endo-siRNAs

To identify potential nuclear RNAi targets, we examined a published list of endo-22GRNAs (supplemental material in Gu et al. [2009]) for those that map to genes known to be expressed in AWC neurons. Our non-exhaustive list (*odr-1*, *tax-6*, *unc-40*, *osm-3*, *odr-4* and *unc-116*) was used as a starting point to design probes for quantifying specific siRNAs. *odr-1* and *tax-6* were examined as each have been implicated in adaptation: overexpressing the GC, ODR-1, blocked butanone adaptation (L'Etoile and Bargmann, 2000) and loss of the calcineurin,TAX-6, promoted adaptation (Kuhara et al., 2002). *unc-40*, *unc-116*, *odr-4* and *osm-3* were examined because they are each required for general neuronal function (Hedgecock et al., 1990; Patel et al., 1993; Dwyer et al., 1998; Shakir et al., 1993) and could therefore serve as controls for the specificity of siRNA dependent regulation. Many of the siRNAs we examined are annotated in Gu et al., 2009 as being most abundantly expressed in the germline, but we suspected that they might also be present in neurons.

Worm Strains

For a complete list of strains used please consult Extended Experimental Procedures. Bristol N2 was used as the wild-type strain. Alleles used in this study are grouped by chromosome.

LG I: *rde-2*(*ne221*; *pk1657*), *rde-3*(*ne3364*), *rrf-1*(*pk1417*), *drsh-1*(*ok269*), *rrf-2*(*ok210*), *drh-3*(*ne4235*), *ego-1(tm521)*. LG II: *rrf-3*(*pk1426*), *alg-2*(*ok304*), *fbf-1*(*ok91*), *nrde-2*(*gg91*). LG III: *rde-4*(*ne337*), *hpl-2*(*tm1489*), *mut-7*(*pk204*), *nrde-1(gg88)*. LG IV: *eri-1*(*mg366*), *mut-6*(*st702*), *drh-1*(*tm1329*), *drh-2*(*ok951*), *pkg-2(ok966*; *tm3878).* LG V: *rde-1*(*ne219*; *ne300*), *ergo-1(gg98).* X: *nrde-3*(*gg74*). *MAGO12*: *sago-2(tm894) ppw-1(tm914) ppw-2(tm1120) F55A12.1(tm2686) R06C7.1(tm1414)*I*; Y49F6.1(tm1127) ZK1248.7(tm1113) F58G1.1(tm1019)* II*; C16C10.3(tm1200)K12B6.1(tm1195)* III*; T22H9.3(tm1186)* V*; R04A9.2(tm1116)* X. *quintuple*: *ppw-2(tm1120) F55A12.1(tm2686) R06C7.1(tm1414)* I*; ZK1248.7(tm1113)F58G1.1(tm1019)* II.

Plasmid Construction and Transgenic Strains

Promoter Fusions for Cell Expression Analysis

phpl-2. Using a PCR based fusion technique (Hobert, 2002), 4 kb upstream of the HPL-2 start site of translation (isoforms a and b share the same start site) was amplified and linked to a GFP thereby placing the GFP at the N terminus of HPL-2 and the entire genomic DNA of HPL-2 (*K01G5.2b*). The PCR product was inserted into pCRII-TOPO vector by TOPO TA Cloning Kit (Invitrogen). p*mut-7*: Using the same method, 3.3 kb upstream of the start site of translation of MUT-7 was amplified and fused to a previously constructed (see "Cell-specific rescue," below) GFP::MUT-7 cDNA (the *mut-7* cDNA came from yk443, kindly provided by Yuji Kohara). This PCR fusion product was subcloned into TOPO.

Cell-Specific Rescue

HPL-2 in AWC. To construct p*ceh-36*::HPL-2, full-length cDNA from yk659 was amplified by PCR from the yk phage stock using two primers (5′-ACCATGATTACGCCAAGCTC and 5′-GTAAAACGACGGCCAGTGAA within the yk vector so that the MCS could be used) flanking HPL-2a and its SL2 leader sequence. The AWC-specific promoter *ceh-36*^{prom3}, referred to as p*ceh-36* or pAWC, had been placed into pPD95.75 with PstI and BamHI previously (p*ceh-36*^{prom3}*-pPD95.75* a kind gift from Oliver Hobert; Etchberger et al., 2007). The amplified HPL-2a fragment was digested with KpnI at the 3′ end (the other end was blunt as a result of Hi-fidelity Taq PCR) and inserted into p*ceh-36*^{prom3}*-pPD95.75* cut with MscI and KpnI. This un-tagged version of HPL-2a was used for the cell-specific rescue in Figure 1D.

MUT-7 in AWC. To construct p*ceh-36*::MUT-7, full-length cDNA from yk443 was fused in frame and downstream of GFP. This was achieved by PCR amplification of mut-7 cDNA from the yk phage stock. The PCR fusion product was then digested with KpnI and inserted into p*ceh-36*^{prom3}*-pPD95.75* pre-cut with MscI and KpnI. This created GFP::MUT-7 under the AWC-specific promoter.

NRDE-3 in AWC. To construct p*ceh-36*::3XFLAG::GFP::NRDE-3, full-length genomic DNA from the construct of 3XFLAG::GFP::NRDE-3 (a kind gift from S. Kenndy; Guang et al., 2008) was amplified with two primers (5′-GTCAGTGGAGAGGGTG AAGG and 5′-aaaaGAATTCTTATGCCCAAAAGTTGCGTC) containing a partial C-terminal GFP. This PCR product was digested with XhoI and EcoRI and ligated into the p*ceh-36*^{prom3}::3XFLAG plasmid (see "3XFLAG tagged HPL-2," below) pre-cut with the same restriction enzymes. This plasmid was used in Figure 1G.

Heat Shock Rescue

Constructs were generated by placing the full-length cDNA encoding HPL-2 or MUT-7, from the corresponding yk clones under the *hsp-16.2* heat-shock promoter (Stringham et al., 1992). cDNA was PCR amplified, and the blunt-end product was ligated into the EcoRV site of the pPD119.16 (1995 Fire vector kit).

AWC-Specific Expression of Histone H3.3 and JMJD-2

HIS-71::GFP (H3.3, a kind gift from Siew Loon Ooi and Steven Henikoff [Ooi et al., 2006]) was PCR amplified. The product was digested with KpnI and SmaI and inserted between the KpnI and MscI sites of the p*ceh-36*^{prom3}*-pPD95.75* plasmid. Full-length cDNA encoding JMJD-2 (yk328) was amplified with primers that contained NcoI and XmaI sites. The PCR product and p*ceh-36*^{prom3}*-pPD95.*75 plasmid were digested with NcoI and XmaI and ligated together. This placed HIS-71 or JMJD-2 under the AWC-specific p*ceh-36* promoter.

Site-Directed Mutagenesis

HPL-2. Site-directed mutagenesis of HPL-2 was performed on p*ceh-36*::GFP::HPL-2a. p*ceh-36*::GFP::HPL-2 was constructed by a PCR based fusion technique to fuse pPD95.75 derived *gfp* in frame upstream of the *hpl-2a* transcript (from yk659). The PCR fragment was digested with KpnI and inserted into p*ceh-36*^{prom3}*-pPD95.*75 pre-cut with MscI and KpnI.

MUT-7. Site-directed mutagenesis of MUT-7 was performed on p*ceh-36*::GFP::MUT-7 (see "MUT-7 in AWC," above).

All site-directed mutagenesis reactions were performed by the QuikChange Site-Directed Mutagenesis Kit and QuikChange Multi Site-Directed Mutagenesis Kit (Stratagene, 200519 and 200515). Primers listed in Table S2 were designed by primerX software (http://www.bioinformatics.org/primerx/).

Bacterial Expression of HPL-2

To construct pET28c::6XHIS::HPL-2 for expression protein in *E. coli*, the *hpl-2* cDNA was amplified from p*ceh36*::HPL-2 with two primers containing a NheI and a XhoI restriction enzyme site at the 5′ end of the forward and reverse primers, respectively (5′-TAG AGCTAGCATGTCGAGCAAATCAACAAAGC and 5′-TAGACTCGAGGAGTGATTAAAGCTCGTCGGC). The PCR product and pET28c (Novagen) were digested with NheI and XhoI and ligated together. pET28c::6XHIS::HPL-2(all S/T-A) was constructed using the same method described above except the PCR template from p*ceh36*::GFP::HPL-2(all S/T-A).

3XFLAG-Tagged Protein Expression in AWC

3XFLAG-Tagged EGL-4. NLS::GFP::EGL-4 was constructed by Lee et al. (2010), and used in Figure 3B for genetic analysis. To construct NLS::3XFLAG::GFP::EGL-4, two pieces of PCR fragments were fused by a PCR based fusion technique (Hobert, 2002). 3XFLAG::GFP was first amplified from 3XFLAG::GFP::NRDE-3 with two primers containing an AgeI site at the 5′ end of the forward primer (5′- aaaaaccggtAGAAAAAATGGACTACAAAGACCATGACGG and 5′-TTTGTATAGTTCATCCATGCCATG). The second PCR containing partial GFP::EGL-4 was amplified from NLS::GFP::EGL-4 with two primers (5′-GTCAGTGGAGAGGGTGAAGG and 5′-AT CATAATATTCCGCTCGGCAAAGATGT). After fusing these two PCR fragments, 3XFLAG::GFP was digested with AgeI and ligated into NLS::GFP::EGL-4 pre-cut with the same enzyme. The correct orientation was confirmed by sequencing. This plasmid was used for the in vitro kinase assay.

3XFLAG-Tagged HPL-2. A 3XFLAG fragment for producing p*ceh-36*^{prom3}::3XFLAG was first amplified from 3XFLAG::GFP::NRDE-3 using two primers (5′- aaaaACCGGTAGAAAAAATGGACTACAAAGACCATGACGG and 5′- TTTGTATAGTTCATCCATGCCATG). The PCR product and p*ceh-36*^{prom3}*-pPD95.75* plasmid were digested with AgeI and NcoI and then ligated together to construct p*ceh-36*^{prom3}::3XFLAG. Next, GFP::HPL-2 was PCR amplified from p*ceh-36*^{prom3}::GFP::HPL-2 with two primers (5′-TGGAAACA TTCTTGGACACAA and 5′-TAGAGAATTCGAGTGATTAAAGCTCGTCGGC) and cut with EcoRI and MfeI. This digested fragment was inserted into p*ceh-36*^{prom3}::3XFLAG pre-cut with EcoRI and MfeI to create p*ceh-36*::3XFLAG::GFP::HPL-2. An *odr-3* promoter was amplified from NLS::GFP::EGL-4 (the original construct is fused to an *odr-3* promoter) by two primers (5′- TGACCATGATT ACGCCAAGC and 5′- aaaaGGTACCCAATCCCTATCTAAAAAAACAATGATCT) and cut with SphI and KpnI. The *ceh-36*^{prom3} promoter was removed from p*ceh36*::3XFLAG::GFP::HPL-2 by cutting SphI and KpnI. To prevent from self-ligation, the digested p*ceh36*::3XFLAG::GFP::HPL-2 was treated with phosphatase by Rapid DNA Dephod & Ligation Kit (Roche) and then ligated with the *odr-3* promoter to create p*odr-3*::3XFLAG::GFP::HPL-2. The final construct was confirmed by DNA sequencing. This p*odr-3*::3XFLAG::GFP::HPL-2 was used for ChIP.

All primers used for creating constructs were designed by primer3 software (http://bioinfo.ut.ee/primer3-0.4.0/primer3/).

Transgenic Lines

All transgenic lines were generated by injecting 20-25 ng/microliter of the constructs along with the co-injection marker a coelomocyte marker p*ofm-1::GFP*(25-50 ng/microliter). The AWC markers p*odr-1::*RFP (30-50 ng/microliter), p*str-2::*RFP (50 ng/microliter) or p*ceh-36*::mcherry (25 ng/microliter) were also part of the injection mix. Heat-shock rescue lines were generated by injecting 2 ng/microliter of the linearized heat-shock constructs digested with ScaI and a mixture of ScaI pre-digested genomic DNA from mutant strains (60 ng/microliter) (Kelly et al., 1997) and a coelomocyte marker *ofm-1::*GFP (25 ng/microliter).

Behavioral Assays

The behavioral assay was conducted as described (Colbert and Bargmann, 1995). Briefly, L4 worms were grown on HB101 for 5-6 days at 20°C and adult animals were collected by washing with 1.5 ml S-basal buffer into 1.5 ml microcentrifuge tubes followed by sedimentation of the worms by gravity. After three washes with S-basal, experimental animals were pre-exposed to 1.5 ml of dilute butanone. Dilution was: 11-12 μl of butanone in 100 ml S-basal. A control population was exposed to buffer and subsequently treated in the same manner as the experimental. Animals were incubated at 20 degrees for 80-90 min while being turned on a Labquake (TM). Animals were washed free of butanone using S-Basal and sedimentation by gravity. After two washes with S-basal, the last wash was with water. Then worms were placed on 10cm chemotaxis assay plates containing 10 ml of 1.6% agar in 5 mM potassium phosphate (pH 6.0), 1 mM $CaCl_2$ and 1 mM $MgSO_4$. 1 μl of butanone diluted 1:1000 in ethanol was applied to a point on the assay plate while 95% ethanol was placed at a spot across from the butanone. 1M sodium azide was placed at the same spots prior to adding butanone and ethanol spots. This anesthetic captures animals that are initially attracted to either substance. Worms were allowed to move for 2 hr and then scored. For all assays, all animals were scored and assays that had a minimum of 50 animals were used in the analysis. Worms were kept at 20°C through all the assay steps.

For heat-shock experiments, worms in their original grown plates were exposed at 30°C for 1 hr and then recovered at 20°C for 2 hr prior to behavioral assays. Then the regular assay steps were performed as described above.

Brood Size Assay

To measure the brood size of wild-type, mutants and transgenic strains an L3 hermaphrodite that had been grown at 20°C was picked and placed onto a plate, which was then incubated at 25°C. Once it had grown to adulthood and its first day's worth of eggs had been laid, animals were gently transferred to fresh OP50-seeded plates and allowed to continue laying eggs. This step was repeated every day until the worm stopped laying eggs. After removing the parent, the plates were incubated another two days at 25°C to allow all eggs to hatch. Larvae and adults were scored to calculate the brood size. Three to four animals' broods were analyzed in three separate experiments (n = 9).

Kinase Assay with Nuclear EGL-4

5 plates of adult animals expressing 2XNLS::3XFLAG::EGL-4 were collected by washing twice with S-basal, once with water and finally with IP buffer. Worms were lysed either by ten strokes in a stainless steel dounce or by flash freezing in liquid nitrogen followed by grinding frozen pellets in a mortar and pestle on dry ice with IP buffer (20 mM Tris pH 7.5, 200 mM NaCl, 2.5 mM $MgCl_2$, 0.5% NP-40, 10% glycerol, proteinase inhibitor cocktail (Roche) and RNaseOUT [Invitrogen]), followed by sonication 2x 10 s at 20% output. Lysates were spun at 16,000 g for 15 min at 4°C (flocculent floating debris was avoided) and supernatants were pre-cleared with Dynabeads protein G (Invitrogen) overnight at 4°C.

For evaluation of 2xNLS-3XFLAG tagged EGL-4 kinase activity, 100 μg of total worm lysate was directly immunoprecipitated using anti-FLAG M2 magnetic beads (Sigma-Aldrich). Immunoprecipitates were washed three times with lysis buffer and two times with kinase buffer (50 mM Tris-HCl pH 7.5, 10 mM $MgCl_2$, 1 mM DTT). Kinase assays were performed directly on the beads for 10 min at 30°C in kinase buffer including 1.5 μg of substrate (HPL-2 WT, HPL-2(all S/T-A), or Histone H1), 2 μCi ^{32}P ATP (PerkinElmer) in the presence of 25 μM cGMP (Sigma-Aldrich). For the evaluation of a commercial PKG's ability to phosphorylate the HPL-2 substrate, 1.5 ng of PKG1α (EMD Millipore) was used as described above. Kinase reactions were stopped by addition of 4X NuPAGE LDS sample buffer (Invitrogen), followed by boiling for 10 min. Half of the samples were electrophoresed on 12% NuPAGE Bis-Tris gels (Invitrogen), stained with Bio-Safe Coomassie stain (Bio-Rad) and the dried gels were analyzed by autoradiography. Quantification of Coomassie stained gels and autoradiographs were performed using a Bio-Rad ChemiDoc XRS+ Molecular Imager equipped with Image Lab software.

Identification of *odr-1* cDNA from Somatic Cells

Although the *odr-1* cDNAs (*R01E6.1a* and *R01E6.1b*) are annotated on WormBase (http://www.wormbase.org/species/c_elegans/gene/WBGene00003848?query=WBGene00003848#04-9eca1-10), the finding that siRNAs are mainly expressed in the germline led to the suspicion that the annotated *odr-1* mRNA might also be germline specific. We required the somatic mRNA species in order to make sure we were able to examine the somatic mRNA using quantitative real-time PCR. To identify somatic mRNA (though possibly not neuronal mRNA, Tim Schedl, personal communication), we extracted total RNA (described below) from sterile *glp-4(bn2)* adults that had been incubated at 25°C from L1-L2s. For the first-strand cDNA synthesis and PCR amplification, we used the 5′/3′ RACE kit, 2nd Generation (Roche). For 3′ RACE, four different PCR forward primers (5′-ATGTGTGTGCTTCGGCTGT, 5′-CACTATC AGGGTTCCGCTTT, 5′-ACCCTCCCGATGATTGTGT, and 5′-GCGAAGACCCCTACCATTTA) were designed using the overlapping sequences of *R01E6.1a* and *R01E6.1b* to generate 4 PCR products. The products were cloned into pGEM-T Easy Vector System I (Promega). 10 clones were sequenced and they shared 100% identity with *R01E6.1b*. Following upon the 3′ RACE results, we designed another three *R01E6.1b* specific reverse primers (5′-TCCAATCCACATCGTTTTCA, 5′-CCCACCAGAGCATAAGAACC, and 5′-CGCTGGCAACATTTCATTTA) for 5′ RACE. 13 clones were sequenced and each had sequences identical to *R01E6.1b* except 60 nucleotides were missing from the 5′ end of the second exon. We were unable to obtain *odr-1* cDNA clones using either SL1 or SL2 *trans*-spliced leader sequences for 5′ RACE.

Isolation of NRDE-3-Associated Small RNA

50-60 plates of adult animals expressing 3XFLAG::GFP::NRDE-3 were collected by washing with S-basal and the population was split in half and then one half was incubated with S-Basal alone and the other half with S-Basal plus butanone for 80 min. Then ~100 animals from each half were used in a behavioral assay as described previously. When examining N2 genetic background, we only used populations that showed wild-type naive CI and an adapted CI of 0-0.3 in NRDE-3 immunoprecipitation. Precipitation was performed as described in Guang et al., 2008. Crude lysates were made by shearing harvested animals with ten strokes in a stainless steel dounce with IP buffer on ice (lysis was verified microscopically). The lysates were sonicated 2x 10 s at 20% output on ice and cleared by centrifugation at 16,000 g for 15 min at 4°C. Supernatants were pre-cleared with Dynabeads protein G (Invitrogen) (1-4 hr 4°C) and incubated with anti-FLAG M2 Magnetic beads (Sigma) for 3-4 hr at 4°C. Beads were washed five times with ice-cold IP buffer and the final rinse was performed at room temperature. FLAG tagged NRDE-3 was eluted with 100ug/ml 3XFLAG peptide (Sigma). Elutates were treated with 4 volume of TRIzol reagent (Invitrogen) and RNAs were eluted by miRNeasy Micro kit (QIAGEN). NRDE-3 associated 22G RNAs were quantified by quantitative real-time PCR in Figure 2D as described below.

Isolation of HPL-2-Associated DNA

p*odr-3*::3XFLAG::GFP::HPL-2 was injected into wild-type animals and the subsequent transgenic line was integrated into the genome by trimethylpsoralen (TMP) (Yandell et al., 1994), followed by outcrossing five times with wild-type animals. 50-60 plates

of adult animals were harvested by washing with S-basal and ~100 animals were applied to a behavioral assay as previously described. Adapted animals with chemotaxis index (CI) of 0.05-0.3 were used in chromatin immunoprecipitation (ChIP) as described (Gerstein et al., 2010). Animals were frozen by dropping small volumes of worm suspension directly into liquid nitrogen. These "popcorns" were then ground in a mortar and pestle on dry ice to create worm powder. Worm powder was incubated in phosphate-buffered saline (PBS) with 1% formaldehyde for 10 min at room temperature (with rocking) and quenched by adding 125 mM glycine for 5 min at room temperature. Worm pellets were washed twice with PBS and once with FA buffer (50 mM HEPES/KOH pH 7.5, 1 mM EDTA, 1% Triton X-100, 0.1% sodium deoxycholate, 150 mM NaCl and protease inhibitors cocktail [Roche]). The pellet was collected by spinning at 3,000 G for 3 min then resuspended in 1.5 ml FA buffer with phosphatase inhibitors and 1% sarkosyl, and sonicated in a Bioruptor water bath according to the manufacturer's recommendations (Diagenode). The homogenate was spun at 13,000 g for 15 min at 4°C and pellet was resuspended in FA buffer and sonicated again. The chromatin extract was collected by centrifugating at 13,000 g for 15 min at 4°C and 20 μl of supernatant was saved as input DNA after RNase and protease treatment and reverse crosslinking as described below. The remaining chromatin extract was pre-cleared with Dynabeads protein G (Invitrogen) and incubated with anti-FLAG M2 Magnetic beads (Sigma) for 3-4 hr at 4°C. Beads were washed twice with FA buffer for 5 min each, once with FA buffer containing 1 M NaCl for 5 min, once with FA buffer containing 500 mM NaCl for 10 min, once with TEL buffer (250 mM LiCl, 1% NP-40, 1% sodium deoxycholate, 1 mM EDTA, 10 mM Tris-HCl, pH 8.0) for 10 min, and twice with TE (10 mM Tris/HCl pH 7.5, 1 mM EDTA) for 5 min. Elution was performed by adding 100ul of elution buffer (50 mM Tris/HCl pH 7.5, 150 mM NaCl, 100ug/ml 3XFLAG peptide [Sigma]) and incubating at 4°C for 30 min (this was performed twice). Eluted immunocomplexes were combined and incubated with 2 μl of RNase A (10 mg/ml) at room temperature for 1 hr. Crosslinks were reversed by heating at 65°C overnight while incubating with 2 μl of proteinase k (10 mg/ml). DNA was purified by Qiaquick PCR purification kit (Oiagen) and used in quantitative real-time PCR in Figure 2E as described below.

Quantitative Real-Time PCR

Preparation of Total RNA

5 plates of adult animals were collected by washing with S-basal and ~100 animals were applied to a behavioral assay plate to perform behavioral assay as previous described. The remaining worms were rinsed three times with M9 buffer and stored at negative 80°C. Total RNA was isolated by TRIZOL extraction (Chomczynski and Sacchi, 1987) from whole animals and purified by 1-bromo-3-chloropropane and precipitated by isopropanol. RNA pellet was resuspended in RNAase-free water and incubated with 1 μl of Turbo DNase I (Ambion) at 37°C for 20-30 min. The reaction was stopped by adding DNase inactivation reagent (Ambion) and RNA was recovered by spinning as recommended by the manufacturer. The total RNA from entire worms was used in 22G RNA and mRNA quantitation in Figures 2B and 2D as described below.

22G RNA Quantitation

The supplemental data from Gu et al. (2009), provided the sequences of all *odr-1* derived 22G RNAs; two sequences including the most abundant species termed odr-1.7 (GCAAACATATTGAGGGTAAGT) and odr-1.6 (ATCTCCTTTTGGACTACCTCG) were used to design Taqman probe and primers for quantization of 22G RNA. The siRNAs isolated from L4 animals from Scott Kennedy's lab provided the sequence of *unc-40* derived 22G RNA (GGATCAGAATCAGAGCAAACGC) for designing Taqman probe and primer. cDNA was generated from 48 ng of total RNA with Multiscribe Reverse Transcriptase (Applied Biosystems). Quantitative real-time PCR reaction mixtures were prepared in triplicate for each sample with a mixture of a fluorogenic probe and TaqMan Universal PCR Master Mix (Applied Biosystems). Thermocycling conditions carried out on a Stratagene's Mx3000P instrument were denaturation at 95°C for 10 min, followed by 40 cycles of 15 s at 95°C and 1 min at 60°C. The threshold cycle number of log-based fluorescence (Ct) was obtained and the relative expression level (ΔCt) of *odr-1* and *unc-40* 22G mRNA was normalized to a mature small nuclear RNA control (sn2343, Applied Biosystems). This control showed little change between naive and odor exposed animal samples. The fold change of *odr-1* and *unc-40* 22G shown on the graphs correspond to the ratio of adapted over naive populations. Populations were only assessed if the animals' behavior indicated they had adapted to the odor.

mRNA Quantitation

For analysis of *odr-1* mRNA, cDNA was synthesized from 1.5 μg of total RNA using iScript cDNA Synthesis Kit (BioRad). Real-time quantitative PCR was performed for 50 cycles (denature at 95°C for 10 min, followed by 50 cycles at 95°C for 30 s, 60°C for 1 min and 72°C for 1 min) in a 25-μl reaction containing 100nM of forward and reverse primers, 2 μl of cDNA, 3 mM of $MgCl_2$ and 12.5 μl of Brilliant SYBR Green qPCR Master Mix (Agilent Technologies). Each sample was prepared in triplicate. The expression level of *odr-1*and *unc-40* mRNA was first normalized to the housekeeping gene *act-3* mRNA whose levels did not change with odor. The primers were used as shown below to determine the Ct value. The fold change of mRNA by odor induced was calculated by the ratio of adapted over naive populations. *odr-1*-mRNA 5′- gcgaagacccctaccattta and 5′- cgctggcaacatttcattta; *unc-40*-mRNA 5′- ggtggaataggtggtcttgg and 5′- cattgggagaggcggagt; *act-3*-mRNA 5′- cggtatgggacagaaggac and 5′- ggaagcgtagagggagagga.

To determine the correlation between the olfactory behavior and *odr-1* mRNA expression, we used Prism4 software to calculate a Pearson correlation. The chemotaxis index of odor-exposed animals and the expression level of *odr-1* mRNA were plotted.

Quantitation of NRDE-3-Associated 22G RNA

NRDE-3 associated 22G RNAs were quantified as described above in "22G RNA quantitation" except that 2 μl of eluted RNA were applied for cDNA synthesis. NRDE-3 associated siRNAs were normalized to IPed X cluster genes (Taqman probe GAAUAG AUACGCGGUAUGAGGU) (Guang et al., 2008) whose levels were not altered with odor.

Quantitation of HPL-2-Associated DNA

To quantify HPL-2 associated DNA, ChIP results were analyzed by qPCR using Brilliant III Ultra-Fast SYBR Green qPCR Master Mix (Agilent Technologies) containing 200nM of forward and reverse primers and 2 μl of eluted DNA in a 20-μl reaction and performed for 40 cycles (denature at 95°C for 3 min, followed by 40 cycles at 95°C for 20 s, 60°C for 20 s). Each sample was prepared in triplicate. The primers were specific to the *odr-1*, *unc-40* or *act-3* locus as shown below. The levels of the housekeeping gene, *act-3* did not change with odor. *odr-1*-A 5′- actcgaggtaataaatgggcatc and 5′- atattgtagtccctgaagtgtgagttaag; *odr-1*-B 5′- cctaacgcaagtgagt atttcctaa and 5′- gtttccttttctaaaatttccagtca; *odr-1*-C 5′- ctcccgaacaggtaggattactta and 5′- gttgtttcaacctgaaatacaaaaa; *unc-40*-A 5′- tagatgtgatgagcgcgttg and 5′- tgtgggtcgcttcctatctt; *unc-40*-B 5′- ttgattacggtacttttttcacgtt and 5′- aatgtgttgtcgaggtctgaaa; *unc-40*-C 5′- catatgagagctggtggtaagtgtt and 5′- accatataatcagaagctggaaataaa; *act-3* 5′- gcccaatccaagagaggtaaata and 5′- actt gagggtaaggatacctgaaa.

We generated a standard curve for each primer product by utilizing known amounts of linearized DNA templates in the qPCR reactions. This allowed us to determine the number of molecules per microliter. This was calculated by the formula: (concentration of DNA; g/μl)/M/N_A where M = weight in Daltons of linearized DNA and N_A = Avogadro's number (6.02×10^{23}). A standard curve was generated by plotting log of molecular number and Ct value in Microsoft Office Excel. All the standard curves were linear and had R-squared values of greater than 0.99 showing the high efficiency of PCR amplification. Thus, the number of molecules of either HPL-2 IPed or input DNA was calculated from its Ct using the respective equation. The IPed DNA was first normalized to the input DNA. The respective ratio of HPL-2 IPed DNA in the total DNA was then normalized to the ratio of HPL-2 IPed *act-3* DNA to input *act-3* DNA in either naive or adapted populations. The final fold change induced by odor was calculated by taking the ratio of adapted to naive values for the input and housekeeping gene normalized DNA.

Genes Tested in Table 1

Mass spectral analysis of the varied Dicer complexes indicated that Dicer associates with the following proteins: ERI-1 (an exoribonuclease) (Kennedy et al., 2004); ERI-3 (novel); ERI-5 (a Tudor domain RNA binding protein) and RRF-3 (RdRP) as well as RDE-1 (an Ago involved in exo-RNAi); ALG-1 and ALG-2 (microRNA Agos); three Dicer-related helicases DRH-1, DRH-2 and DRH-3 (Duchaine et al., 2006; Aoki et al., 2007) and RDE-3 (a beta nucleotidyl transferase) (Duchaine et al., 2006). Genetic evidence also implicated RDE-3 and MUT-7, in exogenous RNAi and endo siRNA biogenesis (Gu et al., 2009). We found that mutants lacking either DRH-2 or RDE-3 were defective for adaptation. This lends evidence to the importance of Dicer-mediated endo-siRNA biogenesis in adaptation.

SUPPLEMENTAL REFERENCES

Chomczynski, P., and Sacchi, N. (1987). Single-step method of RNA isolation by acid guanidinium thiocyanate-phenol-chloroform extraction. Anal. Biochem. *162*, 156–159.

Dwyer, N.D., Troemel, E.R., Sengupta, P., and Bargmann, C.I. (1998). Odorant receptor localization to olfactory cilia is mediated by ODR-4, a novel membrane-associated protein. Cell *93*, 455–466.

Hobert, O. (2002). PCR fusion-based approach to create reporter gene constructs for expression analysis in transgenic C. elegans. Biotechniques *32*, 728–730.

Kelly, W.G., Xu, S., Montgomery, M.K., and Fire, A. (1997). Distinct requirements for somatic and germline expression of a generally expressed Caernorhabditis elegans gene. Genetics *146*, 227–238.

Kuhara, A., Inada, H., Katsura, I., and Mori, I. (2002). Negative regulation and gain control of sensory neurons by the C. elegans calcineurin TAX-6. Neuron *33*, 751–763.

Ooi, S.L., Priess, J.R., and Henikoff, S. (2006). Histone H3.3 variant dynamics in the germline of *Caenorhabditis elegans*. PLoS Genet. *2*, e97.

Patel, N., Thierry-Mieg, D., and Mancillas, J.R. (1993). Cloning by insertional mutagenesis of a cDNA encoding *Caenorhabditis elegans* kinesin heavy chain. Proc. Natl. Acad. Sci. USA *90*, 9181–9185.

Shakir, M.A., Fukushige, T., Yasuda, H., Miwa, J., and Siddiqui, S.S. (1993). C. elegans osm-3 gene mediating osmotic avoidance behaviour encodes a kinesin-like protein. Neuroreport *4*, 891–894.

Yandell, M.D., Edgar, L.G., and Wood, W.B. (1994). Trimethylpsoralen induces small deletion mutations in *Caenorhabditis elegans*. Proc. Natl. Acad. Sci. USA *91*, 1381–1385.

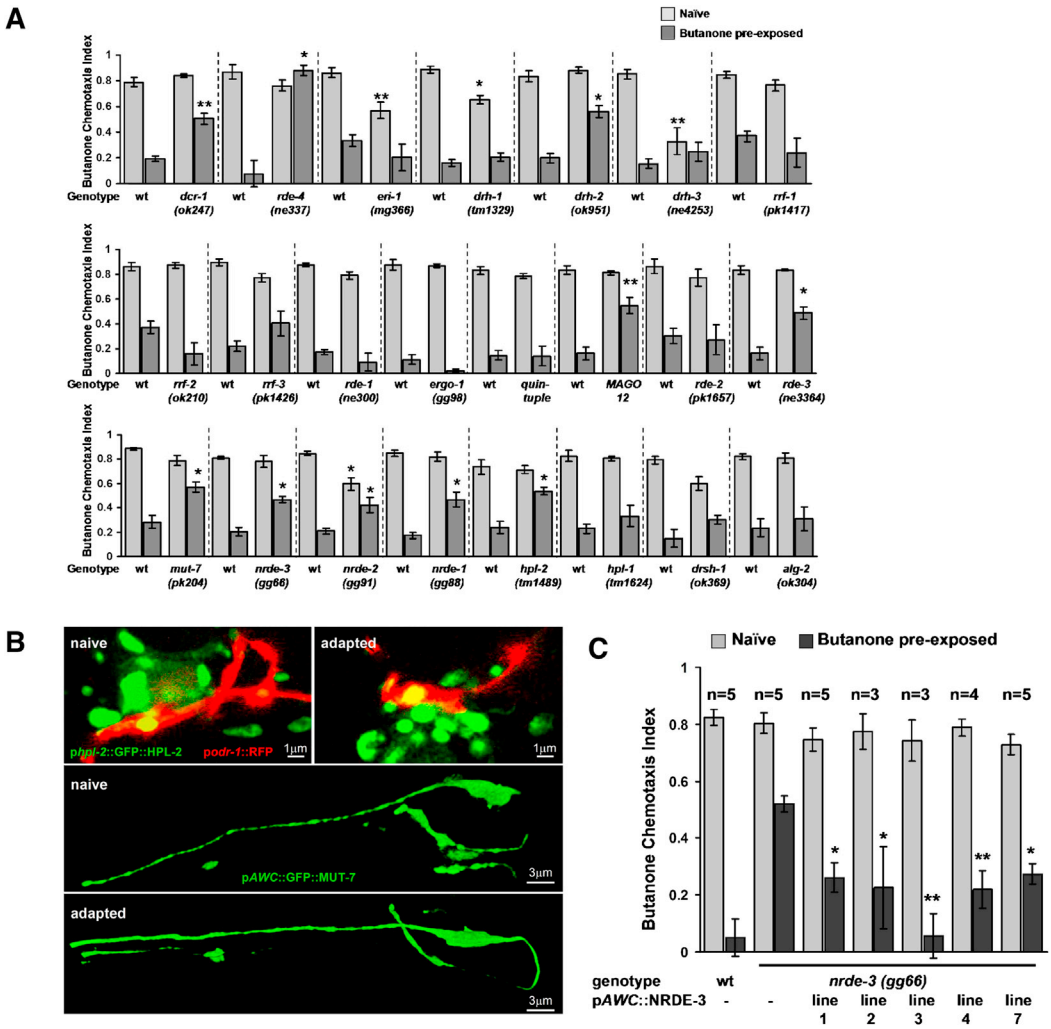

Figure S1. Examining RNAi Defective Strains for Butanone Adaptation, Related to Figure 1

(A) A genetic screen for RNAi defective strains that are also butanone adaptation defective. This is related to Figure 1B and Table 1. Bars represent mean butanone chemotaxis indices of animals that were pre-exposed to either S-basal buffer alone (light gray bars) or butanone diluted in S-basal buffer (dark gray bars) for 80 min before being subjected to butanone chemotaxis assays. The indicated strain was compared to a wild-type control that was grown and assayed in parallel on the same day; error is the SEM. Differences between the CIs of adapted wild-type and mutants were analyzed by paired two-tailed Student t test with equal variance (* indicated < 0.05 and ** indicated < 0.005). *dcr-1(ok247)* and *drsh-1(ok369)* are marked with hT2::GFP(I, III). The animals were assayed on independent days with > 50 animals per assay. *dcr-1(ok247)*, n = 4; *rde-4(ne337)*, n = 3; *eri-1(mg366)*, n = 6; *drh-1(tm1329)*, n = 4; *drh-2(ok951)*, n = 4; *drh-3(ne4253)*, n = 6; *rrf-1(pk1417)*, n = 7; *rrf-2(ok210)*, n = 4; *rrf-3(pk1426)*, n = 8; *rde-1(ne300)*, n = 4; *ergo-1(gg98)*, n = 3; quintuple MAGO, n = 3; MAGO12, n = 3; *rde-2(pk1657)*, n = 4; *rde-3(3364)*, n = 3; *mut-7(pk204)*, n = 4; *nrde-3(gg66)*, n = 4; *nrde-2(gg91)*, n = 5; *nrde-1(gg88)*, n = 5; *hpl-2(tm1489)*, n = 5; *hpl-1(tm1624)*, n = 3; *drsh-1(ok369)*, n = 4; *alg-2(304)*, n = 5.

(B) Odor does not affect the subcellular localization of HPL-2 or MUT-7, related to Figure 1C. (Top) GFP tagged HPL-2 cDNA (short form) was expressed under 3.9 kb of the promoter region in the *hpl-2(tm1489)* mutant background. The transgenic animals were incubated with S Basal buffer alone (naive; left) or S Basal buffer containing butanone (adapted; right) for 80 min before imaging. The AWC neuron was marked by expression of p*odr-1*::DsRed and HPL-2 was only observed in the nucleus. No change in the compact nuclear appearance of GFP tagged HPL-2 was observed after odor-exposure. (Bottom) GFP fused MUT-7 cDNA was expressed under the AWC specific promoter (p*ceh-36*^{prom3}) in *mut-7(pk204)* mutant strains. The confocal images of naive (upper) and odor-exposed (lower) transgenic animals were captured. MUT-7 was expressed throughout the entire AWC neuron and this was not altered with odor exposure.

(C) Individual lines expressing NRDE-3 in AWC rescue the adaptation defects of *nrde-3(gg66)*. This figure is related to Figure 1G. The mean CIs of naive and butanone pre-exposed strains are shown. *nrde-3(gg66)* mutant strains carrying transgenic arrays expressing NRDE-3 under the AWC specific p*odr-3*^{PROM3} were tested alongside wild-type and *nrde-3(gg66)* parental strains. All transgenic lines were created by independent injections. Differences between adapted animals of *nrde-3(gg66)* and the individual transgenic lines were analyzed by two-tailed t test. * indicates $p < 0.05$ and ** indicates $p < 0.005$. Line 4 is shown in Figure 1G.

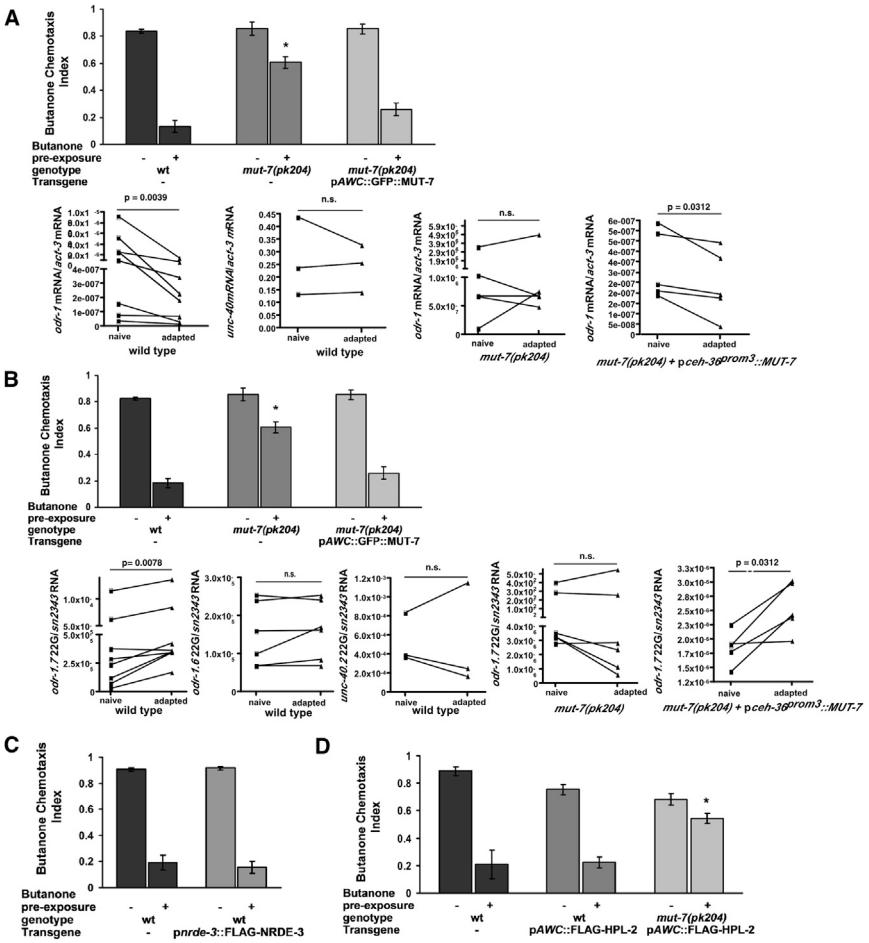

Figure S2. Changes in odr-1-Derived RNA Species in Adaptation, Related to Figure 2

(A) Prolonged odor exposure decreases *odr-1* mRNA levels, related to Figure 2B. (Top) Bars represent the mean chemotaxis indices for the populations that were used in the *odr-1* mRNA analyses in Figures 2B and 2C. Each chemotaxis assay was performed with > 100 animals that had been removed from the rest of the population before it was processed for RNA. (Bottom) Pairwise comparison between the normalized expression level of *odr-1* mRNA (*odr-1* mRNA molecules per *act-3* mRNA molecule) from buffer exposed (naive, squares) and odor exposed (adapted, triangles) populations. A single population of animals that were grown at the same time was split in half and used in the paired analysis. The genotypes compared are wild-type; *mut-7(pk204)* and *mut-7(pk204)*;Exp*ceh-36*^{prom3}::MUT-7. Of note, *act-3* mRNA levels were not altered by odor exposure. To allow comparison between wild-type and *mut-7* as well as the AWC-specific rescue of *mut-7*, the *y* axis for the middle and right pairs was expanded; the units remain the same (*odr-1* mRNA/*act-3* mRNA). P values were obtained by using a one-tailed Wilcox signed rank test of paired medians.

(B) Prolonged odor exposure increases *odr-1* 22G RNA, related to Figure 2D. (Top) Bars represent the mean chemotaxis indices for the populations used in the *odr-1* 22G RNA analyses in Figure 2D (bars 1-5). As can be seen, p*AWC*::GFP::MUT-7 rescued the *mut-7(pk204)* strain's adaptation defects. (Bottom) Pairwise comparison of levels of *odr-1* (odr-1.7 and odr-1.6) *unc-40* (unc-40.2) derived 22G RNAs from population of animals that showed adaptation to butanone. Expression of 22G RNA was quantified by quantitative real-time PCR with a Taqman probe and normalized to an endogenous sn2343 gene whose levels did not change with odor treatment. The normalized expression of each butanone-exposed population (triangles) was compared with its buffer-exposed (squares) control that was grown at the same time and on the same plates and was part of the same initial population. A line links the 22G values of each paired population. Different genotypes are compared: left, wild-type pairs; middle, *mut-7(pk204)* pairs, right, *mut-7(pk204)*;Exp*ceh-36*^{prom3}::MUT-7 (MUT-7 expressed in AWC) pairs. To allow comparison between wild-type and *mut-7* as well as the AWC-specific rescue of *mut-7*, the "y" axis for the middle and right pairs was expanded; the units remain the same (*odr-1*22G RNA/10^7 sn2343). Note: the two very high values for *odr-1siRNA* in graph #4 from *mut-7(pk204)* resulted when we used miRNeasy Micro kit (QIAGEN) rather than the isopropanol precipitation that was used for the other samples.

(C) Olfactory behavioral assay results for populations that were analyzed for NRDE-3 co-IP *odr-1* 22G RNA, related to Figure 2D (bars 6-8). Bars represent the mean chemotaxis indices for the populations that were used in the NRDE-3 associated *odr-1* 22G RNA analyses in Figure 2D (bars 6-8). This shows that expression of 3XFLAG tagged NRDE-3 in wild-type animals does not alter their olfactory behavior.

(D) Bars represent the mean chemotaxis indices for the populations that were used in Figure 2E in which p*odr-3*::3X FLAG::HPL-2 was expressed in wild-type or *mut-7(pk204)* animals. p*odr-3* drives expression in AWB, AWC and AWA neurons and this expression does not alter behavior in wild-type or *mut-7(pk204)* animals. HPL-2 associated DNA was immunoprecipitated from the populations indicated. * indicates two-tailed t test $p < 0.05$ for adapted CIs in wild-type and *mut-7(pk204)* animals with transgenes.

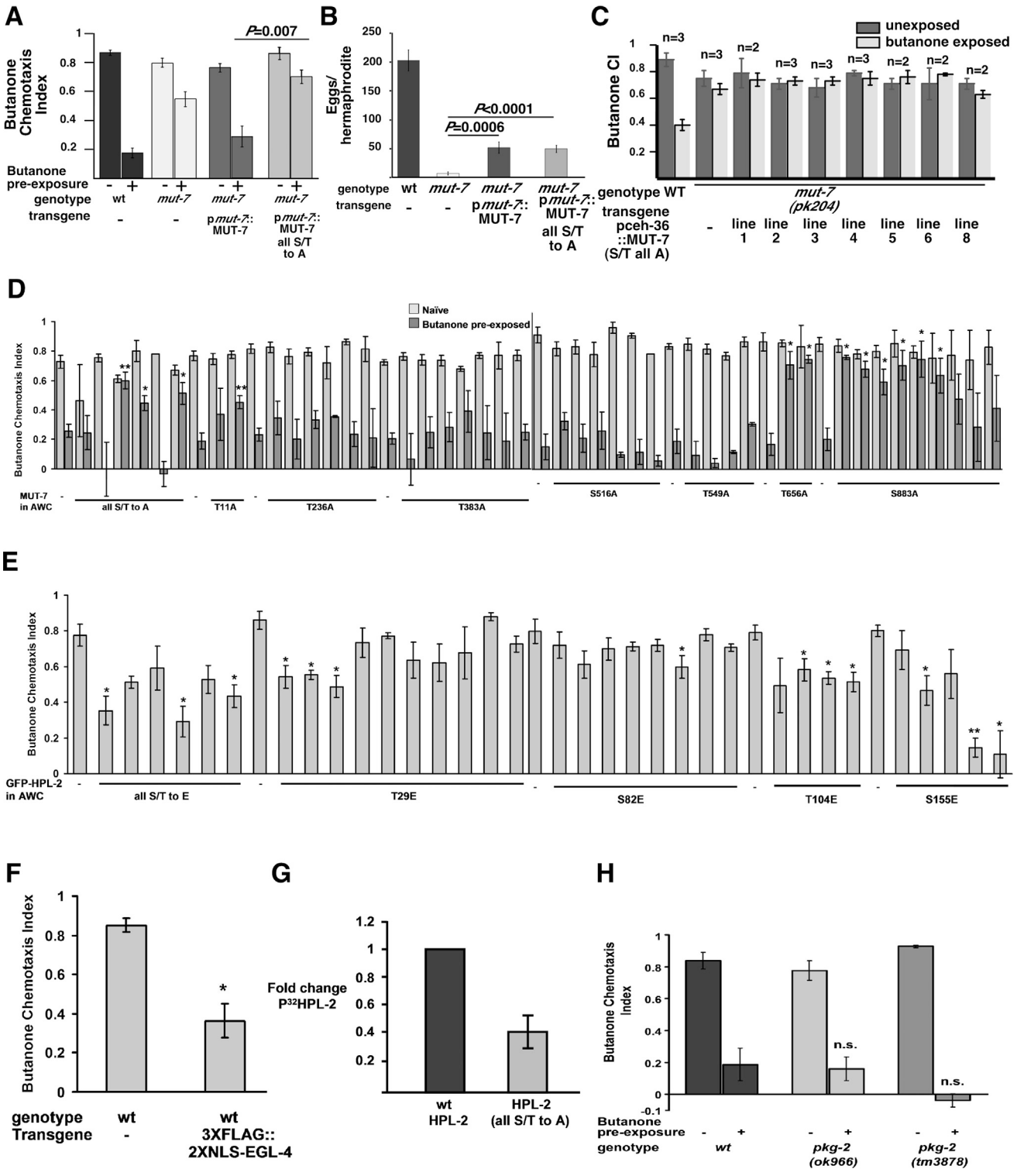

Figure S3. Phosphorylation of HPL-2 and MUT-7 at PKG Consensus Sites Is Required for Adaptation, Related to Figure 4

(A) Alanine substitutions of all PKG consensus sites fail to rescue *mut-7(pk204)* adaptation defects. Bars represent the mean CIs of butanone naive and exposed animals of the indicated genotypes. *mut-7(pk204)* mutant animals expressing wild-type MUT-7 under the control of 3.2 kb of the *mut-7* promoter region (p*mut-7*) restored adaptation, while *mut-7* mutants failed to adapt to butanone when they expressed p*mut-7*::MUT-7(all 7 PKG sites mutated into alanine) (compare 3rd and 4th pairs of bars). Error bars represent the SEM. p values are from two-tailed Student's t test.

(legend continued on next page)

(B) Alanine substitutions of all PKG consensus sites rescue the brood size defects of *mut-7(pk204)*. Bars represent the mean he number of eggs produced by 9 hermaphrodites of the same transgenic lines in Figure S3A were counted. Animals were kept at 25°C and brood size was determined in 3 independent experiments. The defects of the brood size in *mut-7* mutant backgrounds were partially rescued to the same extent whether wild-type MUT-7 or MUT-7 with alanine mutations was expressed (compared 3rd to 4th bars). Bars represent means and error bars are SEM, p values are from two-tailed Student's t test.

(C) Individual lines expressing MUT-7(S/T all A) mutants in *mut-7(pk204)* all fail to rescue the adaptation defects of *mut-7*. All lines were tested in parallel with wild type and *mut-7(pk204)*. The mean value of CIs from the number of independent assay days marked above each strain are represented by the bars. Error bars represent the SEM. p values are from two-tailed Student's t test.

(D) A genetic screen for PKG sites within MUT-7 that are required for adaptation - related to figure 4B. Bars represent the mean butanone chemotaxis index of wild type (N2) animals expressing various forms of GFP-tagged MUT-7 from the AWC specific p*ceh-36*^{PROM3} that had been exposed to buffer (light bars) or butanone in buffer (dark bars) for 80 minutes before the assay. The PKG consensus sites in MUT-7 that were changed from serine (S) or threonine (T) to alanine (A) are indicated below each group of bars. Each group of bars represents independent lines. (-) indicates N2 without a transgene. When all sites were changed (all S/T to A) 3/5 lines failed to adapt as determined by the adapted CI being significantly higher than N2. The lines that had a naive CI lower than 0.5 are not included in the analysis. Thus, 1/2 lines expressing MUT-7(T11A), 0/6 lines expressing MUT-7(T236A), 0/7 expressing MUT-7(T383A), 0/6 expressing MUT-7(S516A), 0/4 expressing MUT-7(T549A) and 2/2 expressing MUT-7(T656A) and 6/9 MUT-7(S883A) failed to adapt to butanone. This suggests that MUT-7 is likely to require phosphorylation at these sites to function in adaptation. Each line was analyzed $n \geq 2$ with >100 adult animals each assay. Error bars represent the SEM. p values are from two-tailed Student's t test. * indicates $p<0.05$ of two-tailed Student t-test between butanone exposed wild type and transgenic animals and ** indicates $p<0.005$ significant difference.

(E) A genetic screen for PKG sites within HPL-2 that are sufficient to induce adaptation-like behavior in the absence of odor- related to 4E. All or four individual serines (S) and threonines (T) within the HPL-2's PKG sites were changed to glutamic acid (E) in the GFP-tagged HPL-2a cDNA. 20 ng/μl of each plasmid was introduced into wild-type animals and individual transgenic animals deriving from independent injections were analyzed for their ability to chemotaxis towards butanone. The bars represent the mean CIs of >3 independent days for each indicated line. Several lines carrying HPL-2(T29E) or HPL-2(T104E) show mild chemotaxis defects, while two lines with HPL-2(S155E) show more severe chemotaxis defects. The PKG site at S155 in the chromo shadow domain is likely to play a key residue for EGL-4 phosphorylation. Two-Tailed t-test were performed by analyzing CIs of unexposed wild type and transgenic animals from at least three independent assays each line and * indicates $p<0.05$ and ** indicates $p<0.05$. The lines used in Figure 5E were: all, line 1; T29E, line 2; S82E, line 4; T104E line 3; S155E line 4. Error bars represent the SEM. p values are from two-tailed Student's t test.

(F) 3XFLAG::NLS::EGL-4 is active as judged by its ability to promote adaptation in naive animals, related to Figure 4D. 2XNLS FLAG tagged EGL-4 were expressed in wild type animals. These naive animals were analyzed for their chemotaxis to butanone. Bars represent the mean values from >3 independent assays. As can be seen, animals expressing nuclear EGL-4 caused chemotaxis defects. The gain-of-function animals were harvested and EGL-4 was purified from whole worm extracts by FLAG immunoprecipitation. These extracts were used *in vitro* kinase assays in Figure 4D.

(G) HPL-2 is phosphorylated at consensus PKG sites by a commercial bovine cGMP-dependent protein kinase. We wanted to determine whether the PKG consensus sites in HPL-2 that we had identified as being important for adaptation are substrates for a well characterized, purified kinase rather than being the result of phosphorylation by a kinase that might co-purify with 3XFLAG-EGL-4. To do this, we incubated 2 ng of PKG1α (EMD Millipore) with 1.5 micrograms of wild type or mutant HPL-2 in our standard assay. Graph is the quantification of two independent kinase assays. The error bars represent mean ± SEM ($p = 0.03$; two-tailed t test). The amount of phosphorylated ^{32}P ATP substrates were normalized to their respective Coomassie stained bands. Values shown for mutant HPL-2 substrate are shown as fold reduction of phosphorylation relative to HPL2-WT set to 1. At least half the signal in wild type represents phosphorylation at the identified PKG sites, indicating that these sites are *bona fide* PKG phosphorylation sites.

(H) EGL-4 is the only PKG required for adaptation of the AWC chemosensory response, related to figure 4. *C09G4.2* was predicted to translate a cGMP-dependent protein kinase (PKG) in *C. elegans*. This second *C. elegans* PKG is called *pkg-2*. To investigate if PKG-2 acts in the AWC neurons, two deletion alleles, *ok966* and *tm3878*, were analyzed for their ability to adapt to butanone. *pkg-2(ok966)* and *pkg-2(tm3878)* each were able to adapt to butanone as well as the wild type strain. All error bars represent SEM and assays were performed on ≥ 3 separate days with > 100 animals per assay. A GFP reporter construct with 2 kb upstream of the predicted ATG start codon of *pkg-2* is expressed in >15 head neurons, none of which was AWC neurons (A. Gupta and N.D.L., unpublished data).